THE JOURNAL OF PHYSICAL CHEMISTRY Letters

Perspective

pubs.acs.org/JPCL

# Pt-Based Core–Shell Catalyst Architectures for Oxygen Fuel Cell Electrodes

Mehtap Oezaslan,*[,†,§] Frédéric Hasché,[†,‡] and Peter Strasser*[,†]

[†]The Electrochemical Energy, Catalysis, and Materials Science Laboratory, Department of Chemistry, Chemical Engineering Division, Technische Universität Berlin, 10623 Berlin, Germany

[‡]Lehrstuhl für Technische Elektrochemie, Fakultät für Chemie, Technische Universität München, 85748 Garching, Germany

**ABSTRACT:** Pt-based core–shell nanoparticles have emerged as a promising generation of highly active electrocatalysts to accelerate the sluggish kinetics of oxygen reduction reaction (ORR) in fuel cell systems. Their electronic and structural properties can be easily tailored by modifying the Pt shell thickness, core composition, diameter, and shape; this results in significant improvements of activity and durability over state-of-the-art pure Pt catalysts. Prompted by the relevance of efficient and robust ORR catalysts for electrochemical energy conversion, this Perspective reviews several concepts and selected recent developments in the exploration of the structure and composition of core–shell nanoparticles. Addressing current achievements and challenges in the preparation as well as microscopic and spectroscopic characterization of core–shell nanocatalysts, a concise account of our understanding is provided on how the surface and subsurface structure of multimetallic core–shell nanoparticles affect their reactivity. Finally, perspectives for the large-scale implementation of core–shell catalysts in polymer exchange membrane fuel cells are discussed.

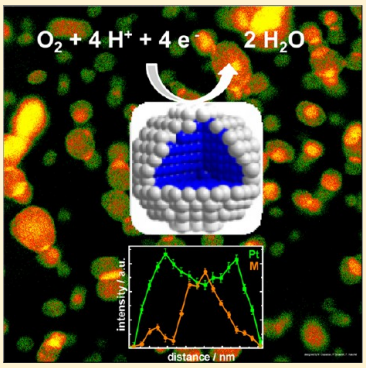


Improvements of activity, selectivity, and durability for nanocatalysts have a great impact on the economic competitiveness of catalytic process. In the last two decades, polymer electrolyte membrane fuel cells (PEMFCs) captured worldwide attention as a promising renewable emission-free technology to meet the increasing demand for clean and efficient power for stationary and transportation applications. Currently, platinum nanoparticles are the most used cathode electrode materials to catalyze the sluggish oxygen reduction reaction (ORR, $O_2 + 4\ H^+ + 4\ e^- \rightarrow 2\ H_2O$) to water in PEMFC systems. The catalytic activity on pure platinum nanocatalysts, however, still requires high metal loadings to meet technical requirements. The critical issues for the utilization of pure Pt catalysts are the high material costs, insufficient catalytic activity, and gradual loss of catalytically active surface area over time due to the electrochemical instability of Pt, particle growth, particle detachment, and carbon corrosion under operating fuel cell conditions. Therefore, the great challenge of today's fuel cell research continues to be the development of efficient and robust cathode electrocatalysts with reduced costs, especially for the automotive sector.

A state-of-the-art membrane electrode assembly (MEA) used in PEMFCs requires a total Pt loading of about 0.5 mg $cm_{geo}^{-2}$.[1−3] Over the past years, the anode loading for the hydrogen oxidation reaction (HOR, $H_2 \rightarrow 2\ H^+ + 2\ e^-$) could be reduced down to 0.05 $mg_{Pt}\ cm_{geo}^{-2}$ without activity loss;[4] yet, the cathode still needs current Pt loadings of around 0.4 $mg_{Pt}\ cm_{geo}^{-2}$. Guidelines and recommendations for PEMFC cathode electrocatalysts used for the commercial implementation in PEMFC vehicles are given from the U.S. Department of Energy (DoE),[5,6] Japanese New Energy and Industrial Technology Development Organization (NEDO),[7] and other worldwide organizations.[8] For instance, the technical targets for PEMFC cathode electrocatalysts proposed from the DoE for 2017 are a Pt-based mass activity of >0.44 A $mg_{Pt}^{-1}$ at 0.90 $V_{iR\text{-}free}$, catalyst loading of 0.125 $mg_{PGM}\ cm^{-2}$ (PGM: platinum group metal), and cost per power for a fuel cell stack of 15 \$ $kW^{-1}$. In regards to the required stability targets, the loss in catalytic activity cannot be higher than 40% after 5000 h of operation. In other words, the requirement for the catalytic activity of ORR electrocatalysts is to increase at least 4–5 fold compared to that for state-of-the-art Pt nanocatalysts.[9−12]

Improvements in activity and durability for electrocatalysts are only achieved by better understanding of the ORR kinetics and its mechanisms as well as catalyst degradation mechanisms under operating fuel cell conditions. The development of DFT-based theoretical predictions of efficient ORR catalysts provided progress in our understanding of ORR activity and yielded promising catalyst materials for fuel cell experimentalists.[13−18] On the basis of these a number of novel electrocatalyst concepts have been prepared and tested in fuel cell laboratories over the past years.

Many of the PGM-containing catalyst concepts are based on Pt alloys in a highly dispersed nanoscale, mostly supported format.[9,11] Only the nanostructured extended thin film (NSTF) electrocatalyst concept prepared by 3M[11,19] has shown higher

**Received:** July 9, 2013
**Accepted:** September 12, 2013
**Published:** September 12, 2013

intrinsic ORR activity as well as reduced active surface area over the time under operating fuel cell conditions compared with alloy nanoparticles. Alloying of Pt with other metals provides experimental parameters to control and optimize the atomic and electronic catalyst structure toward improved ORR performance. Pt alloys with transition metals such as Cu, Co, Ni, and Fe have attracted great attention due to the enhanced ORR activities at reduced content of precious metals.[20−22] In 1998, Toda et al. reported surface-oriented studies of various Pt alloy catalysts, showing an activity increase up to 2× over pure Pt.[23,24] Nowadays, the ORR activities of Pt alloy nanoparticles are significantly superior to that of pure Pt, ranging up to improvement factors of 6−10[25−32] over pure Pt particles in acidic and alkaline environments. This increase was realized by improved synthetic methods coupled with deeper understanding about the kinetic barriers of the ORR mechanism. In particular, Pt-based core−shell nanoparticle architectures have emerged as a promising paradigm to meet and exceed the required activity targets for automotive industries.

The catalyst concept of a bimetallic Pt core−shell nanoparticle is characterized by a Pt-enriched particle shell surrounding a metal core consisting of a pure metal or alloy.

Preparation techniques for core−shell nanocatalysts offer experimental parameters to control the nanoscale structure and composition, including Pt shell thickness, composition of the core, particle size, and particle shape.

Preparation techniques for core−shell nanocatalysts offer experimental parameters to control the nanoscale structure and composition, including Pt shell thickness, composition of the core, particle size, and particle shape. Optimizing these critical characteristics can result in considerable activity and durability benefits. The origin of activity benefits of core−shell nanoparticles is found in altered electronic and geometric properties associated with beneficial chemisorption properties of surface atoms for the minimization of free-energy barriers. DFT works have shown that modified chemisorption properties for adsorbed oxygen species on a Pt-rich surface are largely caused by short-range electronic charge-transfer effects (ligand effects[33,34]) and long-range geometric lattice strain (geometric effects[34]). These electronic and geometric effects result in a shift of the energetic center of Pt-projected d states affecting surface adsorbate bond strengths and thus lead to altered chemisorption of reactants, intermediates, and products. According to the theoretical calculations, the optimal ORR reactivity is depicted by weakness of the binding energy of oxygen-containing species of around 0.2 eV compared to that of pure Pt.[10,15,16] The negative shift of the chemisorption energy for an outermost Pt-rich surface can be engineered by the presence of other metals in the sublayers. Compressive lattice strain in the Pt shells induced by Pt−Cu alloy particle cores, for instance, lowers the bonding strength of oxygenated adsorbates and causes ORR activity increases.[35,36]

We now know that a detailed knowledge of the structure and composition of both the surface and the subsurface layers is very important for understanding and designing active and durable ORR electro-catalysts. Recent impressive developments of aberration-corrected high-resolution microscopic and element-sensitive spectroscopic techniques have helped to uncover the spatial distribution of dissimilar elements in core−shell nanocatalysts and to correlate their structure with the resulting ORR kinetics.

This Perspective gives an overview of recent developments in the area of core−shell ORR electrocatalysts. The overwhelmingly large body of research coupled with its scientific output in this field forces the current Perspective to be highly selective. The first section introduces the critical structural and compositional parameters for tailoring the atomic and electronic structure of core−shell nanocatalysts toward increased activity and durability. The influence of the Pt shell thickness, composition of the core, particle size, and particle shape on the ORR activity and durability will be discussed in this section. An overview of the different approaches and strategies for the preparation of Pt-based core−shell nanocatalysts will be present in the second section. The synthetic approaches vary from (electro)chemical dealloying/leaching methods, reaction processes (segregation tendencies initiated by thermal annealing or by strong surface binding of adsorbates), and deposition methods (heterogeneous colloidal nucleation or underpotential deposition (UPD) followed by galvanic displacement). The third section highlights the great potential by using unique advanced microscopic and spectroscopic techniques to uncover the fine structure and spatial distribution of dissimilar elements in advanced core−shell nanoparticles. Besides ORR activity, long-term durability and chemical stability of core−shell nanocatalysts under real operating fuel cell conditions is addressed (fourth section). Finally, the fifth section discusses some upcoming challenges and future perspectives of the view of the authors to further optimize the state-of-the-art core−shell nanocatalysts. Some other important topics such as commercial Pt catalysts, nonprecious metal catalysts, support materials, Pt-based nanowires and nanotubes, and further extended Pt are outside of the scope of this Perspective but are covered in recent excellent reviews.[2,9−11,37−42]

*Optimizing Structure, Activity, and Stability of Pt-Based Core−Shell Nanocatalysts.* Unlike homogeneously alloyed particles, core−shell particles offer a large variety of structural and compositional parameters, such as Pt shell thickness, composition of the core, particle diameter, and particle shape, toward improved catalytic properties, shown in Figure 1. Understanding of their effects on activity and stability by tailoring the critical parameters is the main key for the design of efficient and robust catalysts.

The Pt shell thickness is a key parameter for controlling the activity of core−shell nanocatalysts. The catalytic properties of the shell are influenced by how much the electronics and geometry of the particle core affect the electronic and atomic structure of the top surface layer. With increasing shell thickness, the intrinsic activity of the core−shell nanocatalysts drops and approaches that of pure Pt nanoparticles. This can be caused either by internal metal leaching or from redeposition of soluble Pt species onto large particles via Ostwald ripening, resulting in particle growth and a drop in the active surface area over time. In both cases, it leads to an alteration of the Pt shell thickness and particle morphology combined with altered activity and stability. Strong ORR activity enhancements were especially observed for Pt shells of a single atomic layer or a few atomic layers. The effects of thickness only on the stability are, yet, more complex depending not only on the particle core and


dx.doi.org/10.1021/jz4014135 | J. Phys. Chem. Lett. 2013, 4, 3273−3291

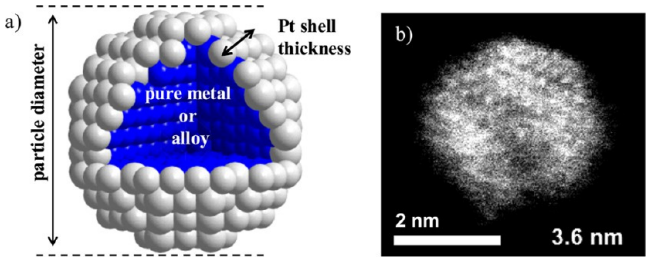


**Figure 1.** (a) 3D cross section of a core−shell nanoparticle. A large variety of experimental parameters can be easily used to optimize the structural and electronic properties of Pt-based core−shell nanoparticle catalysts toward improvements of activity and durability. (b) Visualization of a real catalytically active core−shell nanoparticle using the atomic-resolution HAADF-STEM technique. The core−shell nanoparticle consists of a Co-rich core and a Pt-rich shell. Because there is a significant difference in the atomic numbers of Co ($Z = 27$) and Pt ($Z = 78$), the Pt shell appears brighter than the Co-rich core in this micrograph by virtue of atomic number, or $Z$-contrast. Reprinted from ref 65 with permission of the American Chemical Society, copyright (2012).

size but also on the nature of the support and particle−support interaction.

A deeper understanding of degradation processes of core−shell nanoparticles is crucial to improve their compositional and structural durability and long-term ORR activity.

Another critical parameter for the design of active and durable core−shell nanocatalysts is the composition of the particle core and its chemical stability under operating fuel cell conditions, such as high acid concentration, dissolved molecular oxygen, and highly anodic operating potentials. Metal cores consisting of 3d elements like Fe, Co, Ni, and Cu reveal a stronger increase in ORR activity than those consisting of 4d and 5d elements like Pd and Au.[15,16] The rise in activity is attributed to the weakening of chemisorption energies for reactants, intermediates, and products, which is caused by different d-band energies of dissimilar metals, the resulting acceptor−donator interactions between Pt and the transition metal, as well as the increased lattice mismatch. However, 3d transition metals typically dissolve in contact with strong acids and anodic potentials of up to 1 V/RHE due to their low dissolution potentials. Selective leaching of the nonprecious metal core results in an increase of the Pt shell thickness. The improved ORR activities of core−shell nanoparticles present in the early state of the catalyst life cycle gradually decrease due to the thicker Pt shell and therefore resemble more and more the performance of a pure Pt surface. A complex interplay between the opposite effects of shell thickness and residual nonprecious metal core composition on the activity was shown for Pt−Ni alloy nanoparticles.[31] There, Ni-rich Pt−Ni precursor particles (Pt/Ni, 1:5) resulted in Ni-poor cores combined with thinner shells, while Ni-poor precursors (Pt/Ni, 1:3) showed thicker Pt shells combined with high Ni content in the core. The Ni-rich core material prevailed in activity.

DFT calculations provide information about the structural stability and the surface segregation tendencies of metallic core atoms in various core−shell nanostructures. The stability of the particle core is strongly influenced by the oxyphilic character of the metal, the segregation behavior of the metal atoms from the core induced by temperature, adsorbates, or electrochemical potential conditions, and finally the critical interplay between the dissolution rate of the less noble metal and the diffusion rate of the Pt surface atoms. A large number of various metal and alloy cores have been computationally studied by Balbuena and co-workers.[43−45] Metals with a high affinity for oxygen prefer to migrate on the surface and are immediately dissolved when in contact with acid. Oxygen adsorbs on the catalytic surface by applying anodic potentials. Due to the presence of adsorbed oxygen, the segregation behavior of metals can revert in a core−shell structure, and a borderline behavior of segregation and antisegregation can be observed. Another concept is the utilization of robust transition-metal carbides such as molybdenum carbide ($Mo_2C$) and tungsten carbides (WC and $W_2C$). Due to the "platinum-like" catalytic properties, WC can serve as a particle-like support material for various electrochemical reactions to reduce the amount of Pt and to improve the ORR activity and durability compared to those for pure Pt.[46,47]

As mentioned before, strategies to stabilize the core−shell particles and consequently to improve their catalyst life cycle involve the utilization of metal cores with higher corrosion potential or the utilization of metal cores consisting of an alloy with a relatively high heat of alloying. In fact, recent theoretical and experimental studies on extended polycrystalline surfaces of $Pt_3M$ alloys (with M = Y, Sc, La, Hf) have shown improved ORR-specific surface area activities and stabilities compared to pure Pt and other Pt alloys.[10,15,48] In particular, sputter-cleaned polycrystalline $Pt_5Gd$ showed an impressive resistance behavior up to 1.6 V/RHE.[49] The improved activities and stabilities of Pt rare earth metal alloys are based on a down-shift of the Pt d-band center combined with a more negative heat of alloying. It is assumed that a more negative heat of alloying causes a higher energy barrier to the dissolution of internal rare earth atoms from the Pt alloy catalysts. The preparation of supported nanoscale $Pt_3Y$, $Pt_3Sc$, and $Pt_5Gd$ alloys yet remains a great challenge to date.

The relationship between ORR activity and particle diameter for pure platinum was intensively examined and documented in the literature.[2,50−54] This particle size effect on the activity is based on the geometric and electronic properties of Pt and their adsorption behaviors of oxygenated species on the active sites. The decrease of ORR activity on small nanoparticles originates from the pronounced oxophilic behavior, which leads to a strong binding of oxygen species at low-coordinated Pt atom sites and reduced accessibility of oxygen reactants. Conversely, large monometallic particles show higher intrinsic specific activity as well as enhanced durability due to the reduced driving force to electrochemically dissolve and to coarsen.[28,55−62] In general, the correlation between the electrochemical dissolution rate and potential is explained by the Gibbs−Thomson relation. Large particles show low Gibbs−Thomson energy and consequently a low dissolution rate, while small nanoparticles with a high Gibbs−Thomson energy already electrochemically dissolve at low potentials. A similar trend has been observed for various Pt alloy particles as well. However, for different chemical compositions of alloys, where bulk dissolution of the less noble metal can occur,[63,64] a more complex size−activity relation is apparent. Especially, large alloy particles have a stronger kinetic tendency to form nano-


dx.doi.org/10.1021/jz4014135 | J. Phys. Chem. Lett. 2013, 4, 3273−3291

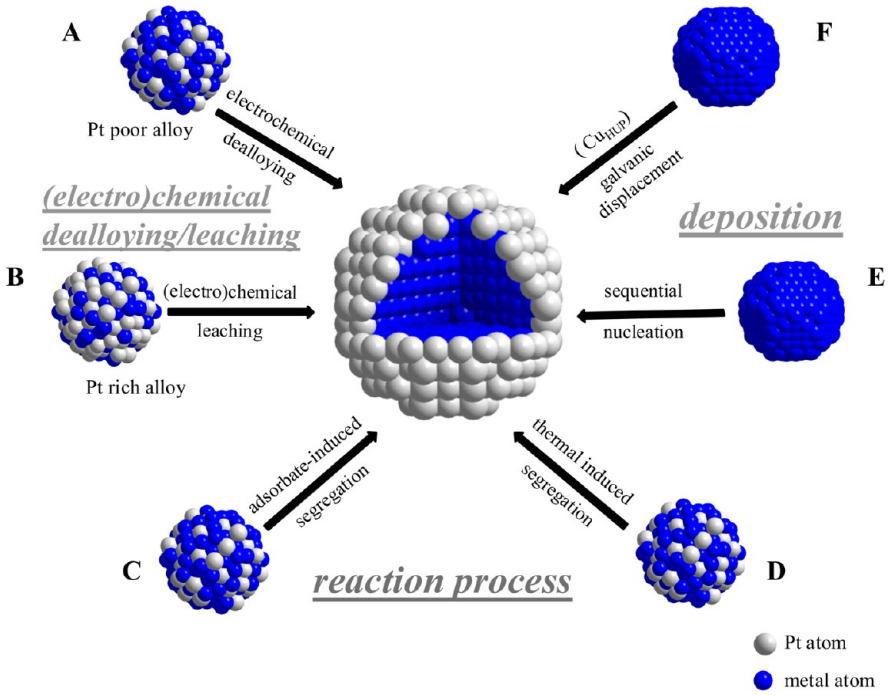


**Figure 2.** Illustration of basic synthesis approaches for the preparation of core–shell nanoparticle catalysts. Electrochemical (acid) dealloying/leaching results in (A) dealloyed Pt bimetallic core–shell nanoparticles and (B) Pt-skeleton core–shell nanoparticles, respectively. Reaction process routes generate segregated Pt skin core–shell nanoparticles induced either by (C) strong binding to adsorbates or (D) thermal annealing. The preparation of (E) heterogeneous colloidal core–shell nanoparticles and (F) Pt monolayer core–shell nanoparticles is via heterogeneous nucleation and UPD followed by galvanic displacement, respectively.

porosity,[29,65,66] which results in a sharp depletion of the nonprecious metal and simultaneously an increase of Pt shell thickness. The thicker Pt shell resembles more and more bulk Pt due to the reduced surface strain and therefore lower intrinsic ORR activity. Hence, the most benefits of activity and stability can be achieved for alloy nanoparticles of a size below 10 nm.

The influence of the surface orientation of pure Pt and Pt alloys on the ORR activity was studied intensively by many research groups under different conditions.[15,67−74] Low-index Pt planes show strong differences in ORR activities.[75] Pt alloy single-crystal surfaces demonstrated that catalytic properties can be strongly enhanced by electronic and structural effects due to the presence of non-Pt-metal-rich subsurface layers. An exceptional 10× activity improvement was experimentally observed for the "skin-type" $Pt_3Ni(111)$ surface compared to a Pt(111) surface. The resulting impressive activity of this $Pt_3Ni(111)$ catalyst originates from the particular compositional oscillation consisting of a pure Pt top layer ("skin") followed by a second Ni-rich layer. To leverage activity and stability enhancements based on the surface orientation, shape-controlled nanoparticles are required.[76] Although the fabrication of shape-controlled monometallic nanoparticles is frequently reported, only a few works on shape-controlled Pt alloy nanoparticles are found in the literature. For instance, $Pt_3Ni$ catalysts with octahedral and truncated octahedral structures showed improvements in ORR activity over that for pure Pt[77−79] yet failed to approach that factor of 10× observed on single-crystal (111) alloy surfaces. More recently, a number of studies have focused on the preparation of octahedral Pt–Ni(111) nanoparticles and have reported activity enhancements of a factor of 10× approaching those observed on single crystals.[32,80,81] It was shown that the careful control of the near-surface composition is crucial in order to bear out this high ORR activity. This explains earlier conflicting results on experimental ORR activities using shape-controlled Pt–Ni octahedra catalysts based on the insufficient information and limited control of the chemical composition of the individual surface facets and the subsurface region. The complex role of facet-specific segregation in shape-controlled particles on the evolving core–shell nanoparticle morphology has recently been demonstrated in octahedrally shaped Pt–Ni ORR particle catalysts.[82] The kinetically controlled enrichment of Ni in the (111) facet centers resulted in a very specific concave-octahedral dealloyed morphology.

In summary, Pt-based core–shell nanocatalysts offer a great potential in tailoring its structural and compositional parameters to optimize their catalytic reactivity and durability. Tuning the Pt shell thickness, composition of the core, particle size, and particle shape enables to adjust optimal synergy interactions of strain and electronic effects toward improved ORR activity and durability for advanced core–shell nanocatalysts.

*Synthetic Strategies toward Pt-Based Core–Shell Nanoparticles.* Versatile and elegant synthesis routes have been developed for the preparation of bimetallic core–shell nanocatalysts. Basically, one metal can (i) deposit onto a second metal as a preformed core, (ii) remove selectively one component from a uniform alloy precursor, or (iii) treat and explore in a way that one metal component within a uniform alloy precursor thermodynamically prefers to segregate toward the surface or into the bulk. A more detailed overview of individual approaches toward the formation of core–shell nanoparticles is illustrated in Figure 2, showing the (electro)chemical dealloying/leaching methods, reaction processes (thermal or adsorbate-induced segregation),


dx.doi.org/10.1021/jz4014135 | J. Phys. Chem. Lett. 2013, 4, 3273−3291

**Table 1. Collection of Different Synthesis Methods for the Preparation of Various Pt-Based Core−Shell Nanoparticles and Their Resulting ORR Activity Improvement Factors Reported in the Literature**

| | | | ORR activity improvement factor[a] | | | |
|---|---|---|---|---|---|---|
| core@shell catalyst | synthesis method[b] | particle size [nm] | Pt mass-based | Pt specific-SA-based | metal precursor salts | refs |
| $PtCu_3$@Pt | A | 3−4 | 6 | 5 | Pt/C, $Cu(NO_3)_2$ | 25,27,65,90 |
| $PtCo_3$@Pt | A | 3−4 | 5 | 4 | Pt/C, $Co(NO_3)_2$ | 25,26,65,92 |
| $PtNi_3$@Pt | A | 6−7 | 7 | 6−7 | Pt/C, $Ni(NO_3)_2$ | 28,134 |
| $Pt_xNi_{1-x}$@Pt | B | ∼5 | | 3−4 | $Pt(acac)_2$, $Ni(acac)_2$ | 95 |
| $Pt_xNi_{1-x}$@Pt | B | ∼5 | | 9 | $Pt(acac)_2$, $Ni(acac)_2$ | 31 |
| $Pt_3Co$@Pt | C | 5 | | 2−3 | $Pt_3Co$ | 104 |
| $Pt_3Co$@Pt | D | 3−9 | | 2−3 | $Pt(acac)_2$,$Co_2(CO)_8$ | 94,96 |
| Au@$Pt_3Fe$ | E | 10 | 4−5 | 3 | $HAuCl_4$, $Pt(acac)_2$,$Fe(CO)_5$ | 107 |
| $Co_{rich}$@$Pt_{rich}$ | E | 4 | 1.5 | 2 | $Pt(acac)_2$,$Co_2(CO)_8$ | 106 |
| $Ir_2Re$/Pd@Pt | F | 3−4 | 3 | | $Ir_2Re$/C, $PdCl_2$, $K_2PtCl_4$ | 121 |
| Pd@$Pt_{ML}$ | F | 4 | 5−6 | 2 | Pd/C, $K_2PtCl_4$ | 117 |

[a]ORR improvement factors were determined by comparison of Pt mass-based activity ($i$(mass)/A $mg_{Pt}^{-1}$) or Pt specific-surface-area-based activity ($i$(specific)/$\mu$A $cm_{Pt}^{-2}$) with those for pure Pt catalyst with comparable particle size at identical reaction conditions and reference potentials, taken from the same paper. [b]Synthesis methods: A = electrochemical dealloying; B = chemical (acid) leaching; C = adsorbate-induced segregation process; D = thermal-induced segregation process; E = heterogeneous colloidal synthesis; and F = underpotential Cu deposition followed by galvanic displacement.

and deposition methods (heterogeneous colloidal nucleation or UPD of Cu followed by galvanic displacement).

Furthermore, the experimentally observed activities of Pt-based core−shell nanoparticle catalysts from a selected set of reports are summarized in Table 1. A direct comparison of catalytic activities across published data is very difficult due to the various catalyst characteristics, reaction conditions, laboratory setups, and reference potentials. These critical issues hinder a comprehensive comparison between the worldwide fuel cell research groups. Therefore, carbon-supported pure Pt nanoparticle catalysts with comparable particle size at identical reaction conditions obtained directly from the same publication were taken to establish ORR improvement factors for Pt mass-based activity ($i$(mass)/A $mg_{Pt}^{-1}$) and Pt specific surface-area-based activity ($i$(specific)/$\mu$A $cm_{Pt}^{-2}$).

The synthesis routes A and B in Figure 2 highlight the chemical leaching and electrochemical dealloying methods. This approach is principally based on the distinct dissolution potentials of dissimilar metals. Dealloying and acidic leaching (or selective dissolution) can be distinguished from each other as two distinctly different atomic processes. In general, dealloying is the electrochemical dissolution of the less noble metal from a uniform multimetallic alloy in acid. A strong depletion of the less noble metal results from the dealloying process, leading to the formation of a thicker Pt-enriched surface consisting of several atomic layers. In contrast, acid leaching only attacks the near-surface region of the alloyed material. Fundamental insight into selective leaching and the initial dealloying process has been intensively studied on extended surfaces of bimetallic single crystals using modern spectroscopic X-ray techniques, which enables a correlation between the different surface stain states, various initial alloy compositions, and the metallic character of different alloys such as Cu−Pt,[83,84] Pt−Ni,[85] Cu−Au,[86,87] and Cu−Pd.[88,89] Recently, the electrochemical dealloying of $PtM_3$ (M = Cu, Co, Ni) alloy precursor nanoparticles (route A in Figure 2) has emerged as a facile synthesis route to form core−shell nanocatalysts with strong enhancement of ORR activity for acidic and alkaline PEMFCs.[25−28,30,31,35,65,90,91] The uniform $PtM_3$ alloy precursor nanoparticles can be prepared by a wet impregnation−annealing method and by a colloidal solvothermal method. A high degree and quality of chemical homogeneity inside of the nanoparticles are still necessary to correlate the structure and chemical composition with the resulting catalytic activity. Therefore, the thermal annealing is frequently applied to prepare homogenously alloyed nanoparticles or to remove surfactants and residual surface compounds. However, nanoparticles show a distinctly different dynamic behavior of alloy formation during annealing compared to that for the corresponding macroscopic alloys. The complexity of the dynamics of alloy formation and crystallinity and their high mobility of particles to migrate and grow on the support material during annealing and reduction make it difficult to design alloy particles with the desired crystal structure, composition, and size. Recent studies on nanoalloy formation and particle growth probed by in situ high-temperature X-ray diffraction help to provide robust preparation of uniform alloy nanoparticles with desired crystal structure, chemical composition, and particle size.[60,92,93] Unlike the impregnation−annealing approach, the organic solvothermal synthesis is more suitable for the fabrication of monodisperse nanoparticles in a large size range at relatively low temperature.[29,31,32,94−97] The preparation of monodisperse metallic nanoparticles requires a fast nucleation step followed by a gradual growth rate on the existing nuclei, captured by the LaMer's model.[98,99] Nevertheless, starting from Pt-poor alloy precursor nanoparticles, the core−shell nanostructure is in-situ-generated by selectively electrochemical dissolution of the less noble metal. The dealloyed particles show a Pt-enriched shell of several atomic layers surrounding a Pt poor alloy core, referred to as the "dealloyed Pt bimetallic core−shell nanoparticles". The origin of the improved ORR activity is due to the lattice strain in the Pt-rich shell, which weakens the chemisorption energies of adsorbed key oxygen-containing intermediates.[35,36,100]

Route B in Figure 2 illustrates the formation of core−shell nanoparticles by acidic and/or electrochemical leaching. Once in contact with acid, the nonprecious metal atoms immediately dissolve from the near-surface region and leave behind vacancies in Pt alloys. Thereby, fast-diffusing Pt atoms gradually enrich the surface, whereas the particle center remains largely unaffected. The rough Pt-enriched surface with a high


dx.doi.org/10.1021/jz4014135 | J. Phys. Chem. Lett. 2013, 4, 3273−3291

concentration of defects is referred to in the literature as a "Pt skeleton" structure.[73,95] The activity improvement of the Pt skeleton particles for ORR is based on the concentration of a less noble metal in the subsurfaces and the extent of low-coordinated Pt surface atoms. During the voltage cycling, small Pt-skeleton-like alloy particles gradually dissolve due to their relatively high Gibbs−Thomson energy and can be partially redeposited via Ostwald ripening on larger Pt-skeleton-like alloy particles. The resulting particles after the Ostwald ripening process show structural similarity toward core−shell nanoparticles (referred to as "Pt skeleton core−shell nanoparticles").[101]

Another strategy to fabricate tailored core−shell nanostructures is the segregation process inside of precursor alloy particles initiated by thermal annealing or by strong surface bonding of adsorbates (adsorbate-induced segregation), such as CO, NO, $O_2$, and $H_2$ (see routes C and D in Figure 2). Surface segregation of atoms is thermodynamically favored by the decrease of heats of mixing.[16,102] Reversibility of the surface reaction restructuring of Pd−Rh alloy particles in different oxidizing and reducing environments could be impressively demonstrated by Tao et al.[103] Under an oxidizing gas like NO, Rh atoms segregate toward the surface of the Pd−Rh alloy, and subsequently, in the presence of a reducing gas like CO, Rh can be diffused back in the particle core. Nevertheless, the segregated Pt-enriched surface is referred to as "Pt skin core−shell nanoparticles" in the literature. The evolved Pt skin protects the subsurface for gradual dissolution of the less noble metal in an acidic electrochemical environment.[72,73] For instance, after CO annealing, the $Pt_3Co$ alloy results in nanoparticles with a Pt-enriched surface and a $Pt_xCo_y$ alloy core due to the strong binding of CO on Pt surface atoms and reduced total surface energy.[104] On the macroscopic scale, the segregation behavior of extended alloyed surfaces was frequently studied by many research groups under different conditions. The macroscopically thermodynamic predictions about their segregation tendencies yet cannot be directly transferred to nanoscale alloys due to the discrepancies in the heat of segregation and surface mixing energy.[105] To predict the near-surface structure and surface composition of segregated bimetallic nanoparticles, Monto Carlo (MC) simulations have recently been used. On the basis of the MC calculations, $Pt_3Co$ nanoparticles revealed a strong correlation between the annealing temperature, particle surface relaxation, segregation, and catalytic properties.[94]

Finally, deposition strategies are also applied to prepare core−shell nanoparticles. They involve the heterogeneous colloidal nucleation and the UPD of Cu followed by galvanic displacement (see routes E and F in Figure 2, respectively). In the colloidal synthesis, platinum can be deposited in the form of a monolayer as well as multilayer shell on other metal particle cores or seeds. This approach provides a controlled fabrication of monodisperse core−shell nanoparticles (referred to as "heterogeneous colloidal core−shell nanoparticles").[106,107] In particular, tuning of the shell thickness can be facilely realized under these conditions. Core−shell nanoparticle examples like Au−Pt,[108,109] Pd−Pt,[110] Cu−Pt,[111] Pt−Cu,[111] and Pt−$Fe_2O_3$[112] are successfully fabricated via colloidal synthesis. Thereby, heterogeneous nucleation and growth processes of dissimilar metals are strongly controlled by interplay between the interfacial energy, surface energy, and strain energy of the lattice mismatch. The lattice mismatch between the metal A, which is growing on existing metal nuclei, and seed B forms due to the different atomic radius and their thermodynamically favored crystalline arrangement. All of these energies can be transferred and translated into so-called "excess energy", which determines the growth mode and particle morphology during the heterogeneous nucleation and growth.[37,113] Detailed information about the excess energy and the effects of the atomic ratio, surface energy, and adsorbates is given in the literature.[114−116] Three classical growth modes are the Volmer−Weber (island growth mode), Stranski−Krastanov (island-on-wetting-layer growth mode), and Frank−van-der-Merwe (layer-by-layer mode) growth. Only the latter growth mode results in uniform core−shell nanoparticles. Metal A prefers to deposit layer-by-layer on an existing particle core or seed consisting of metal B. Surface capping agents and solvents that are used in the early stage of the colloidal synthesis of core−shell nanocatalysts strongly affect the deposition and growth kinetics and subsequently their resulting access of active sites and catalytic properties.

Besides the heterogeneous colloidal nucleation, the deposition of one Pt monolayer on different pure metals and alloys can be realized by UPD of Cu followed by galvanic displacement (see route F in Figure 2). First, a copper monolayer is underpotentially deposited on the surface of mono- or multimetallic particles and serves as a sacrificial monolayer for the subsequent displacement of platinum to form a monolayer shell (referred to as "Pt monolayer core−shell nanoparticles"). The UPD is well-known for the electrochemical deposition of metal A onto a metal B substrate at a potential that is slightly less negative than the equilibrium potential of metal A. In particular, Adzic and co-workers as well as other research groups have shown huge spectra toward the preparation and engineering of a catalytically active Pt monolayer on different metal and alloy cores for various electrochemical reactions.[117−124] Due to the very thin Pt shell in the form of one monolayer, the Pt monolayer core−shell nanoparticles show a very high Pt-based mass activity for ORR. Some works showed that the pretreatment step with Cu UPD on the existing core is not always necessary to form a Pt shell.[125,126] Galvanic displacement reaction between Pt ions and an existing less noble metallic surface also fabricates core−shell nanoparticles, denoted as "Pt-decorated core−shell nanoparticles". The difference between the standard potential values of Pt and the other used metal is adequate for the displacement reaction to be both thermodynamically as well as kinetically favorable. Although the galvanic displacement reaction only occurs on the surface, the Pt shell thickness is not fairly controlled. To protect the morphological structure of the existing less noble metal core, mild conditions must be adjusted for the galvanic displacement for Pt.

Furthermore, the physical vapor deposition method was broadly used by surface scientists to prepare bimetallic alloy and/or core−shell nanoparticles.[127−133] Under vacuum and at elevated temperature, the deposition of a pure vaporized metal onto a support material occurs by condensation. The thermal activation leads to the surface diffusion and sintering of the deposited metal atoms. The formation of bimetallic nanoparticles is yet highly complex and is influenced by the thermodynamic characteristics of the bonding between both metals and segregation-induced processes and by the kinetics of the surface diffusion, sintering, and heterogeneous nucleation determined by defect sites as well as by the experimental parameters, such as deposition time, sequence, elevated temperature, and pretreatment of the substrate surface. The


dx.doi.org/10.1021/jz4014135 | J. Phys. Chem. Lett. 2013, 4, 3273−3291

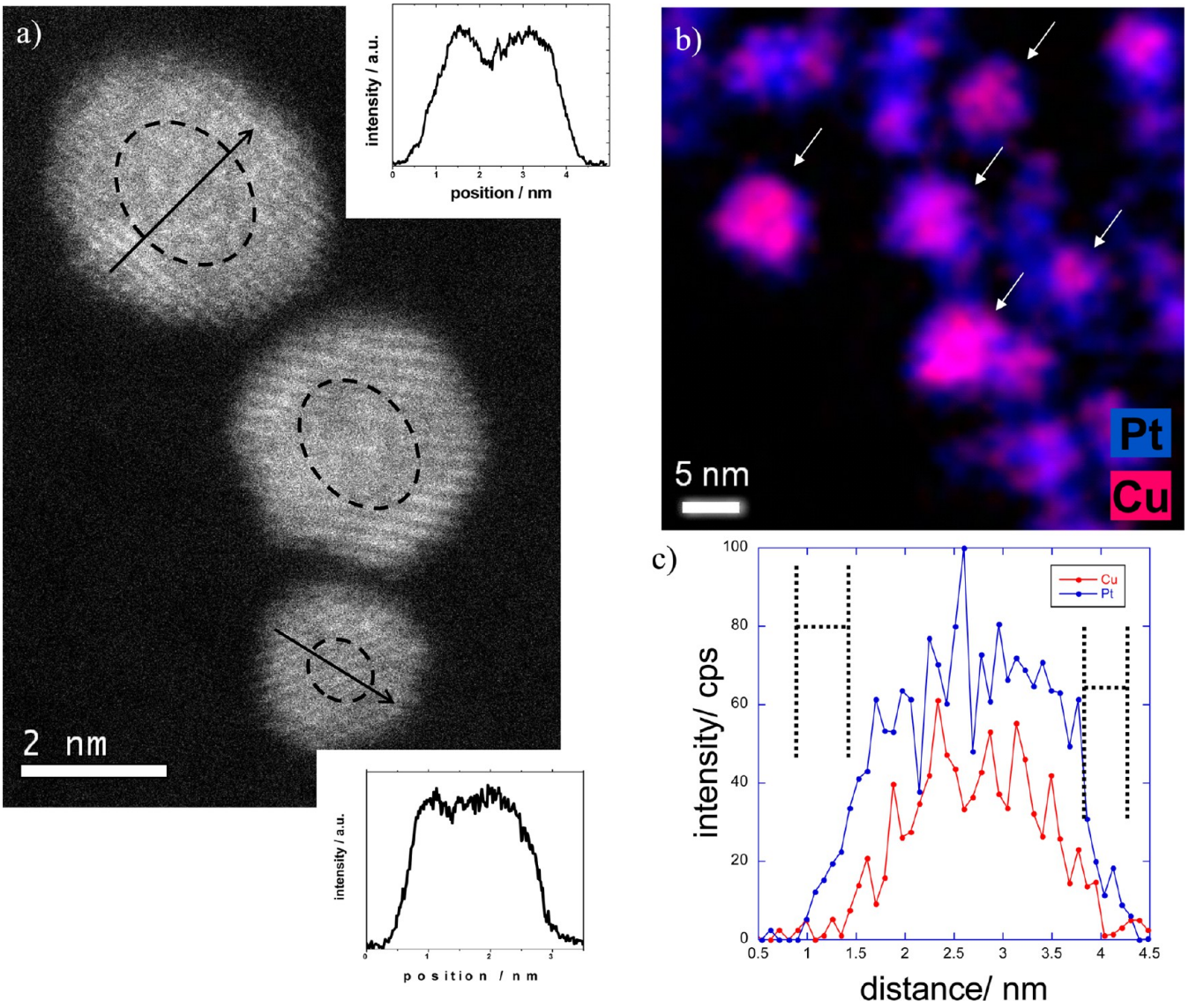


**Figure 3.** (a) High-resolution HAADF-STEM micrograph of representative dealloyed $PtCu_3$ core−shell nanoparticles below 5 nm and the corresponding HAADF intensity line profiles. The black arrow denotes the scan direction of the intensity line profiles. The dashed lines inside of the particles indicate the dark shaded regions. Reprinted from ref 65 with permission of the American Chemical Society, copyright (2012). (b) EDX mapping of dealloyed $PtCu_3$ nanoparticle ensemble, showing the formation of a core−shell nanostructure. (c) High-resolution EDX line profile of a dealloyed $PtCu_3$ nanoparticle below 5 nm, showing a monotone concentration drop of Cu toward the particle surface and a surface enrichment of Pt. Reprinted from ref 35 with permission of Nature Publishing Group, copyright (2010).

most published results about the formation of bimetallic core−shell nanoparticles via vapor deposition showed a broad size distribution and ill-defined composition and structure. Compared to the above-mentioned synthetic approaches for the controlled preparation of core−shell nanoparticles, the vapor deposition method has lost more and more importance.

*Morphology and Composition of Pt-Based Core−Shell Nanocatalysts.* The morphology and composition of core−shell particles are strongly related to their resulting catalytic activities and catalyst lifetime under operating fuel cell conditions. Modern synchrotron spectroscopic and scattering X-ray techniques, such as high-energy photoemission (HE XPS), high-energy X-ray diffraction (HE XRD), anomalous X-ray diffraction (AXRD), anomalous small-angle X-ray diffraction (ASAXS), and X-ray absorption spectroscopy (XAS) have provided a deeper insight into the phase structure, chemical distribution, particle size, and surface lattice strain of nanoscaled core−shell particles.[35,36,135−138] In the last two decades, electrochemical XAS studies have frequently been conducted to monitor in situ the structural evolution of bimetallic systems in real time, including the formation of core−shell structure. Although the in situ XAS technique provides changes in structural and electronic properties of catalysts during electrochemical reaction processes, it is further a bulk average characterization technique for very uniform and homogeneous samples. If the nanoparticles show chemical and structural inhomogeneity, like chemical composition, crystal structure, and size, the information obtained by XAS is largely limited.[139]

In real space, high-resolution high-angle annular dark field scanning transmission electron microscopy (HAADF-STEM) combined with element-sensitive electron energy loss spectroscopy (EELS) or energy-dispersive X-ray spectroscopy (EDX) has provided atomic-scale structural information to understand


dx.doi.org/10.1021/jz4014135 | J. Phys. Chem. Lett. 2013, 4, 3273−3291

and to optimize the catalytic properties of core−shell particles.[140]

Figure 3a shows a high-resolution HAADF-STEM micrograph of individual dealloyed $PtCu_3$ core−shell nanoparticles of below 5 nm in their catalytically mostly active state. In this case, the dealloyed catalytically active particles were prepared by route A shown in Figure 2, so-called electrochemical dealloying.[35,65] The HAADF-STEM micrograph shows for each particle a dark contrast in the center and bright contrast at the particle edge. The intraparticle intensity variation is especially evident by establishing the intensity line profile across the particles. Due to their spherical shape, small dimension, and distinctly different scattering factors of Cu and Pt, the observed intensity variation is largely caused by the compositional heterogeneity within these dealloyed particles. The intraparticle contrast features indicate the formation of a Pt-rich particle shell and Cu-rich alloy core. To corroborate the formation of a core−shell nanostructure, element-sensitive EDX mapping was also performed on the dealloyed Pt−Cu particle ensemble. In Figure 3b, the EDX mapping over the particle ensemble revealed that only the surface of the uniformly alloyed particles was attacked from the dealloying process to form a Pt-enriched shell and a relatively unchanged alloy particle core. The spatially atomic distribution of both elements inside of the particles was well-determined by high-resolution EDX line scanning, as shown Figure 3c. In dealloyed particles, the monotonic drop of the less noble metal toward the surface and a strong surface enrichment of Pt are supported by the high-resolution EDX spectra. On the basis of the microscopic and spectroscopic investigations on dealloyed Pt−Cu bimetallic particles with a diameter of 3−4 nm, the average Pt shell thickness is in the range of 0.5−1.0 nm (2−4 monolayers). This is consistent with small-angle X-ray scattering measurements on the same dealloyed nanoparticles.[36] The core−shell nanostructure was the dominant structural type for dealloyed $PtCu_3$ electrocatalysts of below 10 nm in studies of other groups as well.[141]

Mazumder et al.[142] reported a novel preparation of Pd/Au/PtFe core−shell nanoparticles with tunable multilayer shells using a colloidal synthesis involving oleylamine and oleic acid as capping agents, as shown in route E of Figure 2. Au layers and subsequent PtFe layers were deposited onto the freshly synthesized Pd nanoparticles to obtain controlled multilayer shells. The HAADF-STEM micrograph (Figure 4b) showed an individual multilayer particle with dark shading in the center consisting of pure Pd and bright shading at the edge consisting of Au and PtFe. To corroborate the formation of inner and outer shells of Au and PtFe over Pd particles, element-sensitive EDX line scan measurements were performed. According to the EDX line scan analysis shown in Figure 4c, multimetallic Pd/Au/PtFe core−shell particles with a diameter of 10 nm revealed a thickness of the PtFe outershell of 2.0 ± 0.4 nm, followed by an inner Au shell of 1.1 ± 0.2 nm. Furthermore, the authors demonstrated how the Au shell thickness over the Pd particle core can be fairly tuned under optimized reaction conditions. They found a correlation between the shell thickness and the resulting ORR activity; with decreasing Au thickness, the ORR activity increased. Tailoring of the shell thickness enables one to optimize the synergy interactions of electronic and strain effects between the particle core and shell.

Aside from small core−shell particles in the size range of 2−5 nm, the utilization of larger nanoparticles of >5−10 nm has also received much attention due to their improved intrinsic activity

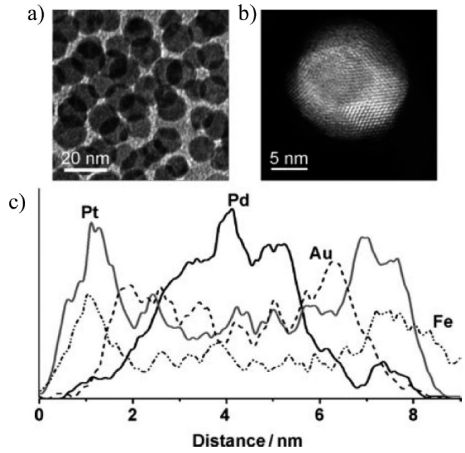


**Figure 4.** (a) TEM and (b) HAADF-STEM micrographs of Pd/Au/PtFe core−shell nanoparticles with multilayer shells consisting of a Au inner shell and PtFe outershell. (c) High-resolution EDX line scan analysis across an individual multilayer core−shell nanoparticle shows the fine structure and internal atomic distribution of the dissimilar elements obtained by scanning 150 points with a beam size of about 2 Å. Reprinted from ref 142 with permission of Angewandte Chemie, International Edition, copyright (2010).

and durability. Interestingly, at large particle size and, in particular, at low initial Pt content, more complex morphological and compositional structures appear in Pt alloy cathode catalysts after the electrochemical and/or acidic treatment. For instance, during leaching of large Pt alloy particles in strongly acidic conditions, percolated, Pt skeleton, or spongy structures were frequently reported in the literature.[72,73,101,143−145] Here, the notation Pt skeleton is distinguished by a surface composition profile showing a strong enrichment of Pt atoms in a much roughened surface region. This morphological type was predominantly observed for alloys with an initial Pt content of approximately >50 atom %. In contrast, Pt alloy particle precursors with a lower initial Pt content result largely in a percolated structure. The percolated structure is characterized by adjacent internal Pt-rich and Pt-poor regions inside of acid-leached particles. Particles having (nano)voids and (nano)pores are designated as spongy structures. The spongy structure is evolved by continuous electrochemical dealloying of percolated particles[101] or by acid leaching of Pt-poor alloy particles.[145] Despite a large number of experimental studies on Pt alloy particle catalysts, a detailed understanding of the effect of particle size, the nature of the crystal phase, the degree of chemical alloy homogeneity, and the nature of metals on the resulting morphological structure and composition of alloy particles is still missing to date. For instance, ordered intermetallic $PtCu_3$ particles with a size of 10−20 nm were treated via two dealloying methods, acid leaching and electrochemical dealloying. The acid-leached particles lost their ordered structure and formed numerous stable voids, while the electrochemical dealloying resulted in Pt skin core−shell particles consisting of a thin Pt-rich shell (3−5 monolayers) and an almost nonattacked ordered core.[145]

The changes of composition and particle size of acid-leached Pt−Co nanoparticle ensembles in postcycled MEA were comprehensively studied by Shao-Horn and co-workers.[144,146] Figure 5a shows a HAADF micrograph of two individual particles after operating in a MEA and their final chemical composition established by EDX. The post-mortem catalyst analysis revealed the existence of two distinct structure types in


dx.doi.org/10.1021/jz4014135 | J. Phys. Chem. Lett. 2013, 4, 3273−3291

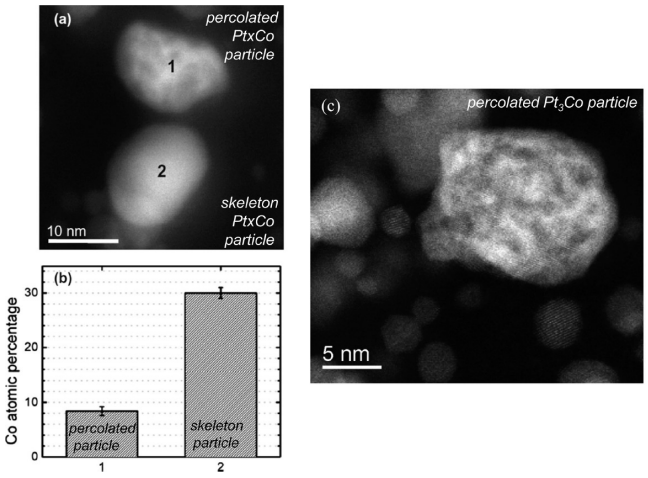


**Figure 5.** (a) HAADF-STEM image and (b) average Co atomic percentage of representative percolated $Pt_xCo$ particles (labeled as 1) and skeleton $Pt_xCo$ particles (labeled as 2) observed in the P-MEA. Error bars in (b) are standard deviations generated by the INCA software. Reprinted from ref 101 with permission of the *Journal of The Electrochemical Society*, copyright (2010). (b) Aberration-corrected HAADF-STEM image of an AT (acid-treated)-"$Pt_3Co$" particle, where large intensity variations are noted. Reprinted from ref 144 with permission of The American Chemical Society, copyright (2009).

Pt−Co particle ensembles, the percolated structure (denoted by (1)) as well as the skeleton structure (denoted by (2)). The experimental observations of both structures in a Pt−Co cathode MEA were explained by the inhomogeneity of the initial composition, the intraparticle homogeneity, and the particle size of the used Pt−Co particles.

Nevertheless, the comparison of the final chemical compositions in single particles showing percolated or skeleton structure established by EDX revealed that the Co content in percolated particles was significantly lower than that in skeleton particles (~6 atom % Co in percolated versus ~30% Co in skeleton particles; see Figure 5b). Figure 5c shows a high-resolution HAADF micrograph of an individual percolated particle with strong intensity variation, indicating the formation of intraparticle regions with high and low Pt content. The evolution of percolated particles with Pt-enriched zones was described by the interplay of electrochemical dissolution rates of the non-noble metal and surface diffusion of remaining Pt atoms. While the less noble metal atoms immediately dissolve by contact with an acid electrolyte, the remaining Pt atoms diffuse on the surface and form clusters with higher coordination number. In this work, it was highlighted that the percolated particles gradually changed their structure and composition during voltage cycling. The Pt-poor regions became more and more pronounced and evolved intraparticle hollow regions, voids, or nanopores due to the successive loss of the less noble metal by dissolution. On the other hand, Pt skeleton nanoparticles transformed into core−shell nanoparticles during voltage cycling.[101] The transfomation into core−shell structure occurred by Pt redeposition. Small alloy

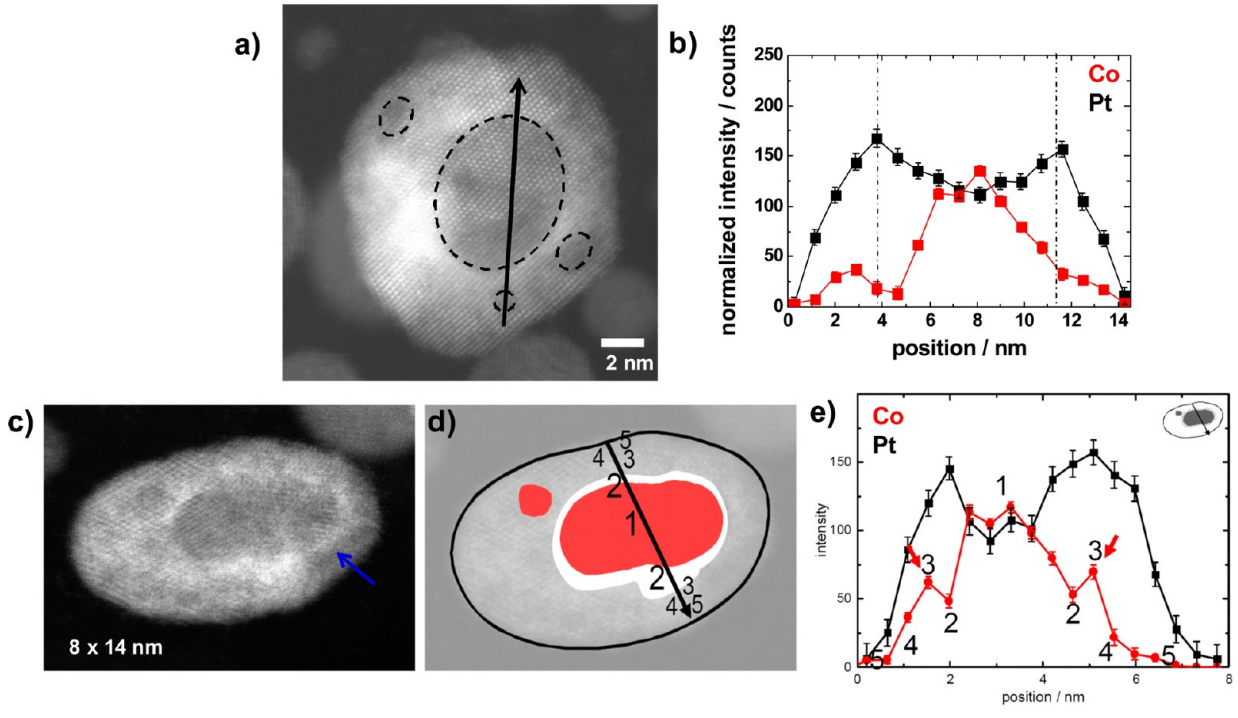


**Figure 6.** (a) High-resolution HAADF micrograph providing *Z*-contrast conditions of a dealloyed Pt−Co bimetallic nanoparticle showing a multiple core−shell structure. At the upper part of the nanoparticle, individual atomic columns are resolved. It is oriented along a $(1\bar{1}0)$ zone axis of the face-centered cubic structure. (b) EELS intensity profiles across the particle for Pt (black squares) and Co (red squares). The EELS profiles are normalized with the elemental scattering factor and hence represent thickness-projected compositions. (c) High-resolution HAADF micrograph, (d) schematic representation, and (e) EELS intensity profile of a dealloyed ellipsoidal Pt−Co particle showing a highly complex self-organized compositional core−shell structure. The red and white region in panel d represents dark and bright contrast features in the HAADF micrograph. These contrast features correspond to the high Co composition in the core (1) and a subsequent depletion zone around the core (2). Red arrows highlight shoulder/plateau features of the Co signal (for the numbers, see the text). Reprinted from ref 147 with permission of The American Chemical Society, copyright (2012).


dx.doi.org/10.1021/jz4014135 | *J. Phys. Chem. Lett.* 2013, 4, 3273−3291

nanoparticles completely electrochemically dissolve and partially redeposit on larger Pt skeleton particles via Ostwald ripening.

Very recently, a comprehensive high-resolution microscopic and element-sensitive spectroscopic investigation on various dealloyed Pt-poor bimetallic electrocatalysts has shown a strong correlation between frequently recurring morphological structures, intraparticle composition, and initial particle size.[65,66,147] This size morphology−composition relation evidences the existence of different morphological structure types for Pt−Cu, Pt−Co, and Pt−Ni particles, which can emerge during chemical dealloying. As shown in Figure 3a, small dealloyed Pt alloy nanoparticles showed a simple core−shell arrangement, prepared via route A of Figure 2. However, with increasing particle size of up to 10−15 nm, the formation of multiple less noble metal-rich cores with irregular shape strongly dominated in dealloyed particles. They constituted a highly complex self-organized structure. Finally, very large particles >30 nm showed clearly morphological nanoporous features typically found in acid corrosion of macroscopic alloy samples.[65] Pore evolution during corrosion has intensively been studied on extended alloyed surfaces. The utilization of advanced in situ and ex situ spectroscopic and microscopic techniques such as surface-sensitive X-ray diffraction, scanning Auger electron microscopy, and others have enabled a better understanding of dealloying process at the atomic scale.[63,64,86,87,148−153] In bimetallic nanoscale alloys, however, where diffusion and metal corrosion typically differ considerably from those in corresponding bulk materials, the detailed mechanism of porosity evolution is still poorly understood. High concentration and high mobility of low-coordinated surface noble metal atoms combined with the surface smoothing for reducing surface energy play an import role for the evolving structure and composition during dealloying.

Figure 6 shows high-resolution HAADF-STEM micrographs and element-sensitive EEL intensity profiles of representative dealloyed Pt−Co nanoparticles with a size range of 10−20 nm. As a guide to the eye, the large dark shaded region in the particle center and the several dark spots of few-nm size in the bright shaded shell region shown in Figure 6a are denoted with dashed lines. The observed contrast features inside of the dealloyed particle indicated a more complex structure and morphology compared to single core−shell nanoparticles showing only one dark shading in the particle center and bright shading at the outermost parts. High-resolution element-sensitive EEL line scan measurements were carried out on these dealloyed self-organized Pt bimetallic particles to uncover the spatial chemical distribution. Across the particle, the corresponding EELS intensity line profiles for Pt and Co (see Figure 6b) revealed that the large dark shaded region in the center and the additional dark spots at the particle shell were strongly correlated with a spatial increase of the Co concentration. On the basis of the spectroscopic and microscopic results, the large dealloyed Pt bimetallic nanoparticles of up to 20 nm showed the presence of multiple less noble-rich cores. Besides the core center, spatial less noble-metal-enriched regions of a few nanometers in the Pt shell regime were uncovered and are referred to as "less noble metal satellites". The authors described the features of multiple cores and satellites by critical interplay between the reducing thermodynamic interfacial energy and highly mobile Pt surface atoms. Beside the existence of multiple less noble-metal-rich cores, fine structure investigation on dealloyed Pt bimetallic nanoparticles of 10−20 nm revealed unusual self-organized compositional profiles, like several subsequent Co-rich and -poor layers in the particle shell region.[147] Figure 6c displays a HAADF micrograph of an individual dealloyed Pt−Co core−shell nanoparticle showing a complex element distribution. It is noted that a thin bright shell surrounds the dark shaded particle core, symbolized with a blue arrow in Figure 6c and with a white area in the sketch in Figure 6d. The different areas inside of the ellipsoidal particle showing distinct intensity contrast features (Figure 6c) were denoted with numbers in the schematic representation (Figure 6d). As shown in Figure 6e, the corresponding EELS line scan across the particle shows a high Co concentration at the center (1) and two additional pronounced off-center Co peaks at ∼1.8 and ∼5 nm (3). In particular, in the thin bright area (2), the Co signal showed minima, indicating a local depletion of the Co concentration several atomic layers below the particle surface. This is clearly different from oscillatory composition profiles observed in the top 3 or so layers of thermally annealed Pt skin bimetallic particles. A detailed fine structure analysis later revealed that the simple description of these particles in terms of single core−shell nanoparticles is insufficient for dealloyed particles with a size of 10−20 nm. Instead, the experimental composition profiles appeared more consistent with the presence of multiple spherical alloy shells surrounding a common metal alloy core. These conclusions were corroborated by very similar self-organized subsurface enrichment profiles observed during the electrochemical dealloying of highly active Pt−Ni alloy nanoparticles.[31] There, dealloyed nanoparticles with an initial Ni content of >50% exhibited two off-center Ni composition maxima, while Ni was minimized near the surface and in the particle center, indicating a spontaneous self-organized formation of Ni-enriched spherical shells at a distance of 1−2 nm below the particle surface.

*Durability Studies of Pt-Based Core−Shell Nanoparticles under Fuel Cell Conditions.* At the beginning of their lifetime, Pt-based core−shell nanocatalysts show considerable ORR activities compared to pure Pt catalysts, meeting and exceeding the activity targets proposed from different institutions.[5] The improved activities are based on their special electronic and geometric properties, such as the Pt shell thickness, composition of the core, particle size, and particle shape. In contrast, the required durability requirements of fuel cell cathode nanocatalysts have been exclusively achieved with so-called nanostructural thin film (NSTF) catalysts.[11,19] These catalysts consist largely of dealloyed extended Pt alloy thin films on a large nanostructured support. Due to their macroscopic dimensions, the formation of porous Pt structures on the surface is likely and leads to an increase of the catalytically active surface area. Achieving the DOE durability targets for carbon-supported core−shell particles, however, remains a key challenge in fuel cell research. A much deeper understanding of the degradation processes for core−shell nanoparticles is necessary to improve their catalyst lifetime at maintaining ORR activity.

In general, the losses of the electrochemically active surface area and catalytic performance are attributed to the particle growth via Ostwald ripening and/or coalescence, particle detachment, carbon corrosion, gradual Pt dissolution, and, in particular, in the case of core−shell nanoparticles, the increase of the Pt shell thickness as well as the depletion of internal metals.[28,39,59,80,101,107,120,141,154,155] Moreover, the fuel cell performance strongly depends on the chosen operating conditions such as potential regimes, upper turning potentials,


dx.doi.org/10.1021/jz4014135 | J. Phys. Chem. Lett. 2013, 4, 3273−3291

**Table 2. Selective Overview of the Stability of Pt-Based Core−Shell Nanocatalysts and Their Resulting Losses of the ECSA and Pt-Based Specific Activity ($i_{specific}$) Depending on the Experimental Parameters, Catalyst System and Particle Size[a]**

| core@shell catalyst | particle size [nm] | technique | accelerated degradation method | accelerated degradation parameters | loss of ECSA/% | loss of specific activity/% | ref |
|---|---|---|---|---|---|---|---|
| $Pd@Pt_{ML}$ | 4 | MEA-25 $cm^2$ | potential cycling | 100 000 cycles; 0.7−0.9 V/RHE; 30 mV/s; 80 °C; 150 $kPa_{abs.}$; 100% RH; $H_2$ and $N_2$ | −42 | +8 | 107 |
| $Pd_9Au_1@Pt_{ML}$ | 5 | MEA-25 $cm^2$ | potential step cycling | 200 000 cycles; 0.6−1.0 V/RHE; 50 mV/s; 80 °C; 150 $kPa_{abs.}$; 100% RH; $H_2$ and $N_2$ | −67 | | 120 |
| $Pt_xCo_{(1-x)}@Pt$ | | MEA-50 $cm^2$ | potential cycling | 30 000 cycles; 0.61−1.01 V/RHE; 50 mV/s; 80 °C; 101 $kPa_{abs.}$; 100% RH; $H_2$ and $N_2$ | | | 120 |
| $PtCu_3@Pt$ | | MEA-50 $cm^2$ | potential cycling | 10 000 cycles; 0.6−1.0 V/RHE; 50 mV/s; 80 °C; 101 $kPa_{abs.}$; 100% RH; $H_2$ and $N_2$ | −35 | −72 | 141 |
| $PtCo_3@Pt$ | | MEA-50 $cm^2$ | potential cycling | 30 000 cycles; 0.61−1.01 V/RHE; 50 mV/s; 80 °C; 101 $kPa_{abs.}$; 100% RH; $H_2$ and $N_2$ | −37 | −3 | 141 |
| $Au@FePt_3$ | 10 | RDE | potential cycling | 60 000 cycles; 0.6−1.1 V/RHE; 50 mV/s; $O_2$-saturated 0.1 M $HClO_4$ | −6 | −7 | 141 |
| $PtCu_3@Pt$ | 3−4 | RDE | potential cycling | 10 000 cycles; 0.5−1.0 V/RHE; 50 mV/s; $N_2$-saturated 0.1 M $HClO_4$ | −6 | −24 | 107 |
| $PtCo_3@Pt$ | 3−4 | RDE | potential cycling | 10 000 cycles; 0.5−1.0 V/RHE; 50 mV/s; $N_2$-saturated 0.1 M $HClO_4$ | +7 | −42 | 59 |
| $PtNi_3@Pt$ | 6−7 | RDE | potential cycling | 10 000 cycles; 0.5−1.0 V/RHE; 50 mV/s; $N_2$-saturated 0.1 M $HClO_4$ | +21 | −47 | 59 |

[a]The resulting losses of ECSA and $i_{specific}$ were established before and after applied accelerated stability protocols, taken from the same paper.

and scan rates. For instance, nanoparticles strongly suffer from the frequent start-and-stop driving of PEMFC vehicles due to the strong metal dissolution and carbon corrosion combined with a strong particle detachment under highly anodic potentials (up to 1.5 V/RHE). A selected set of reports about the experimentally observed losses of the electrochemically active Pt surface area (ECSA) and Pt-based specific surface area ($i_{specific}$) is shown in Table 2.

Again, the utilization of modern advanced microscopic and spectroscopic techniques has helped to uncover the relationship between the reactivity and durability of core−shell nanocatalysts. The changes in the nanostructure, composition, and particle size of catalysts have correlated with the experimentally applied parameters. Figure 7 shows a very impressive parallel electron microscopic investigation by Muller and co-workers,[156] where hundreds of inhomogeneous Pt−Co core−shell nanoparticles were probed after the durability test (0.61−1.01 V/RHE at a sweep rate of 50 mV $s^{-1}$ and 30 000 cycles) to highlight their changes in intraparticle compositional distributions and structure. The acquisition of EELS mappings over hundreds of nanoparticles was realized in a high-speed mode using an increased beam current and wide collection angle. A commercial $Pt_3Co$ nanocatalyst was utilized to examine the different lifetimes during aging under operating fuel cell conditions. This work uncovered a strong correlation between the Pt shell thickness and particle size. An interesting degradation mechanism manifested itself in the existence of two distinctly different morphological particle structure types, that is, single core−shell nanoparticles and multiple core−shell nanoparticles have been shown. The observed increase in mean particle size was largely attributed to a growth of the Pt shell thickness resulting from redeposition of Pt, which formed during the complete dissolution of small particles. Particles with multiple Co-rich cores, however, appeared to have undergone a more complex mechanism; initial coalescence of smaller particles is followed by Pt deposition growth. These multiple core particles showed a stronger increase in Pt shell thickness compared to single core−shell nanoparticles. The authors suggested that due to their larger size of multiple core−shell nanoparticles, Pt redeposition preferentially occurred on such coalesced particles and led to a stronger growth of the Pt shell thickness. This study highlighted an interesting synergy between coalescence and Pt redeposition to explain the stronger increase of Pt shell thickness on coalesced alloy particles.

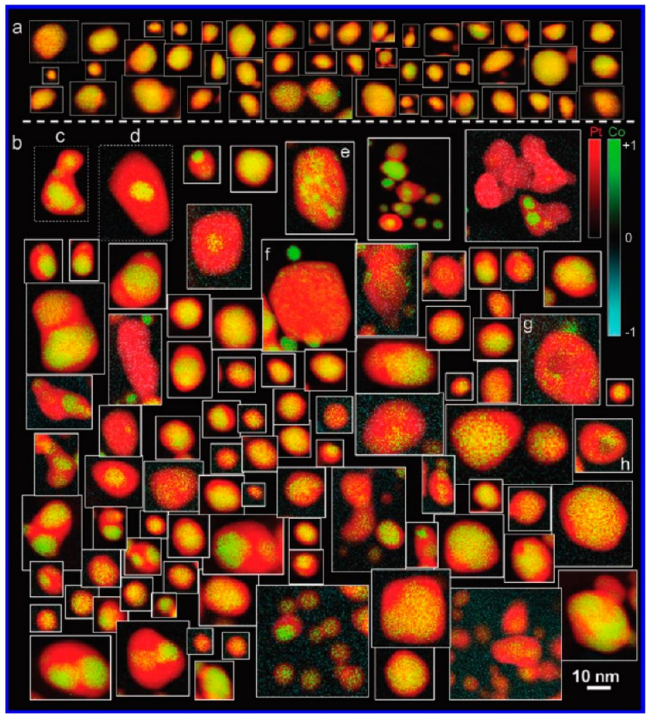


**Figure 7.** Collage of EELS spectroscopic images from the (a) as-received and (b) the voltage-cycled sample. As shown in the color bars, the relative Pt concentration, normalized in each separate image, is plotted in red, and the Co concentration ranges from green to turquoise. Particles (c−h) from the cycled sample are discussed in more detail in the cited paper. Reprint from ref 156 with permission from The American Chemical Society, copyright (2012).


dx.doi.org/10.1021/jz4014135 | J. Phys. Chem. Lett. 2013, 4, 3273−3291

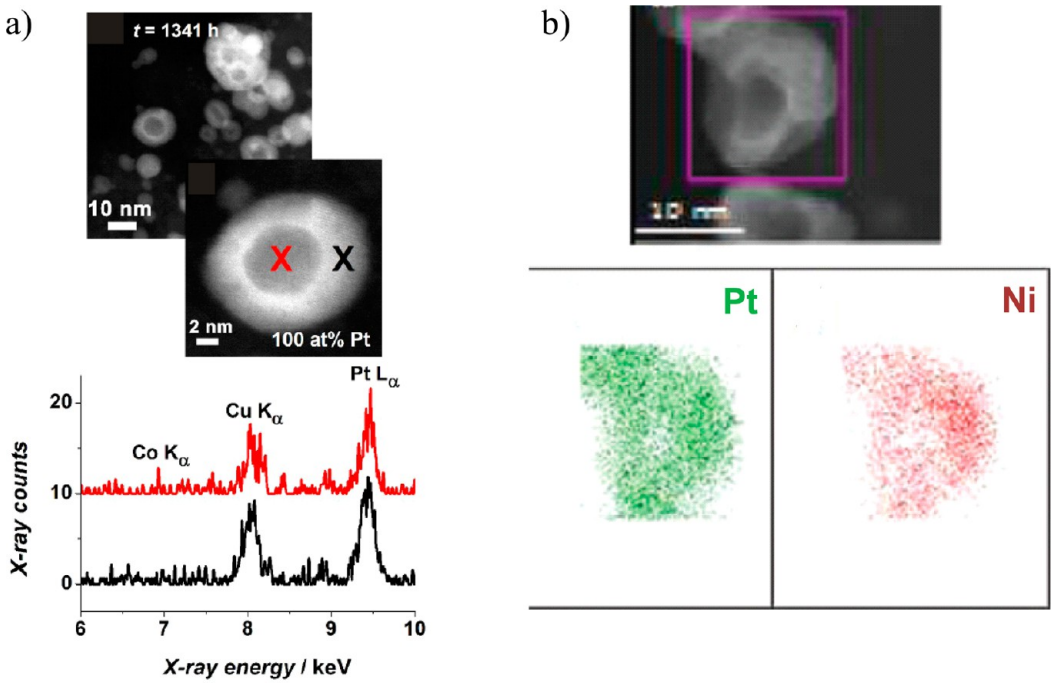


**Figure 8.** (a) Aberration-corrected HAADF images of Pt−Co/C nanoparticles after operation at 20 A ($j$ = 0.24 A cm$^{-2}$) for $t$ = 1341 h. The particle-averaged atom % of Pt and Co are determined by EDX. EDX spectra recorded at the center and at the edge of the particle during a line scan analysis. The crosses in the images indicate the locations of the line scan analysis. The copper signal arises from the copper grid where the catalyst is deposited during TEM measurements. Reprint from ref 157 with permission of Elsevier Limited, copyright (2011). (b) HAADF image of a single nanoparticle used for EDX mapping of the (c) Pt and (d) Ni distribution within the nanoparticle. Colored pixels indicate where the element was detected above the background. Reprinted from ref 80 with permission of The American Chemical Society, copyright (2012).

Influences of the operating conditions on the durability of a PEM fuel cell stack composed of 16× single MEAs consisting of Pt/C at the anode and $Pt_3Co$/C at the cathode were comprehensively examined by Dubau et al.[157] The PEM fuel cell stack was operated at various constant current densities over a long time. The observed loss of catalytic activity under these different conditions was correlated with the changes in structure and chemical composition for the $Pt_3Co$ nanoparticle cathode catalyst. Especially, the treatment at low current density (high cathode potential) led to a strong dissolution of Co atoms in $Pt_3Co$ alloy nanoparticles. In Figure 8a, the HAADF micrographs show contrast features in the nanoparticles after operation at 20 A ($j_{geo}$ = 0.24 A cm$^{-2}$) for 1341 h. Despite the similarities of the HAADF intensity cross profiles with core−shell nanostructures, the EDX analysis clearly revealed that the particles only consisted of almost pure Pt. Therefore, the observed intensity contrast features were related to the changes in intraparticle thickness and not in chemical composition, as shown before. Hollows or voids formed inside of the post-mortem particles due to the almost complete dissolution of the internal less noble metal atoms. The mechanism of the evolution of compact hollow nanoparticles is yet poorly understood to date and is intensively discussed in the literature. In the above-mentioned work, the authors explained the evolution of "hollow" platinum nanoparticles by interplay between fast electrochemical acidic Co dissolution, strong surface segregation of Co induced by adsorption of oxygenated surface species, and the nanoscaled Kirkendall interdiffusion effect. Basically, the Kirkendall effect describes a vacancy-mediated diffusion mechanism based on the different diffusion rates of the single compounds in alloys.[157] The faster-diffusing species move outward and generate a flux of vacancies in the opposite direction to counterbalance the net flux of the faster-diffusing species. Above a distinct concentration, vacancies commence to condense into voids in solid materials. The Kirkendall effect can be initiated by thermal annealing and strong surface binding of adsorbates to form hollow-like structure. Good examples published in the literature are hollow NiP and CoS nanoparticles.[158−161] Another possible explanation for the evolution of hollow nanoparticles is the so-called dealloying mechanism. Dealloying is based on interplay of the different rates of dissolution of less noble metals and surface diffusion of remaining noble metals. The remaining more noble metal atoms diffuse on the surface and form clusters on the surface. The resulting fine nanostructure that forms during dealloying is strongly influenced by the initial alloy composition, particle size, applied potential range, temperature, and additives in the electrolyte.[160,162,163] Although the complex mechanism is highly unclear to date, further studies frequently demonstrated the appearance of these hollow nanoparticles resulting from a simple voltage cycling on Pt alloys. Figure 8b shows HAADF micrographs and EDX mapping of Pt−Ni nanoparticles after 20 000 voltage cycles (between 0.6 and 1.0 V at 50 mV s$^{-1}$).[63,64,149,150,153,164,165] The compositional results obtained from the EDX mapping of postcycled nanoparticles showed a strong dissolution of internal Ni atoms and the evolution of hollow nanoparticles, again. The hollow particles revealed a final composition of around 12−20 atom % Ni. The residual Ni atoms were almost uniformly distributed in the compact particle shell. Another example was reported by Adzic and co-workers.[80] They showed a simple synthesis route for the fabrication of compact hollow Pt nanoparticles by using Ni nanoparticles as a template. Ni nanoparticles were electrodeposited on a carbon support and served as a sacrificial surface


dx.doi.org/10.1021/jz4014135 | J. Phys. Chem. Lett. 2013, 4, 3273−3291

for the subsequent displacement of platinum to form nanoparticles having a Pt-rich shell and a Ni-rich core. The Ni template was then electrochemically dissolved after a few voltage cycles in acid, and only pure Pt nanoparticles remained, showing hollow intraparticle features. In addition, the hollow Pt nanoparticles showed improved ORR activity compared to pure Pt or Pt alloy nanoparticles. The origin of the improved ORR activity in such hollow nanoparticles was hypothesized to be linked to the lattice contraction in the Pt shell even in the absence of other transition metals. Despite their improved initial activity, hollow Pt nanoparticles showed a relatively large particle size compared to single solid Pt particles at similar metal mass. Another aspect is that the inner surface area does not participate in the surface-sensitive reaction and likely blocks the access of active sites. Long-term stability behavior of hollow Pt particles compared to solid Pt nanoparticles of similar size has not been studied to date.

Studies on the temporal sequence of dominant degradation processes for various dealloyed Pt bimetallic core−shell nanocatalysts and pure Pt nanocatalysts were reported by Hasché et al.[28,59] In these works, the dealloyed highly active core−shell nanocatalysts were subjected to two different voltage cycling test (10 000 cycles in the voltage range of 0.5−1.0 V/RHE at 50 mV $s^{-1}$, referred to as the "lifetime" test, and 2000 cycles in the voltage range of 0.5−1.5 V/RHE at 50 mV $s^{-1}$, referred to as the "start-up" test). Both test protocols served as accelerated degradation tests to simulate the long-term behavior of fuel cell electrocatalysts. The loss of surface area and ORR performance over the time were traced by determining the ECSA, changes in initial particle sizes and chemical compositions, as well as the catalyst morphology. They found that all nanocatalysts approached a voltage-dependent quasi-stable (critical) particle size in the first cycle regime. Afterward, additional cycling only led to a little particle growth. The critical particle size that was adjusted during the first cycle regime is strongly dependent on the upper turning potential. They highlighted that for Pt alloys and pure Pt nanocatalysts, the critical particle size was around 3−4 nm in the lifetime test, while in the start-up test, the critical size grew up to 5−7 nm due to the used higher upper turning potential. After the critical particle size was reached, the gradual decay of ECSA curves for pure nanoparticles was largely associated with carbon corrosion and particle detachment as the dominant degradation mechanism. These two distinct time scales of the degradation process (particle growth and dealloying/carbon poison removal followed by support corrosion and particle detachment) are consistent with recent in situ SAXS studies of supported Pt particles.[28,58−61] On the basis of the experimental results, a simple model for the temporal degradation sequence of Pt bimetallic core−shell nanocatalysts was developed, which looks as follows: At the early stages of the catalyst life cycle, the electrochemical dissolution of small particles predominates. Concomitantly, dealloying of the less-noble metal component occurs inside of particles of all sizes. Once small particles completely electrochemically dissolve, Pt redeposition and particle growth via Ostwald ripening commence and control the ECSA loss. The intrinsic activity of the core−shell catalysts over time gradually drops because of the formation of a thicker Pt shell, either due to continued dealloying of the core or due to Pt redeposition on the particle surface. Afterward, the particles reaches a quasi-stable value of size; the successive ECSA loss is controlled by carbon support corrosion combined with particle detachment.

As another strategy toward improved chemical stability of fuel cell cathode catalysts, some research groups focus on core−shell nanocatalysts consisting of precious metals as the core, such as palladium and gold. For instance, Pt monolayer core−shell nanocatalysts with a Pd and/or $Pd_9Au_1$ core and a size of 4−5 nm showed reduced ECSA and activity losses after 100 000 voltage cycles (between 0.7 and 0.9 V/RHE) and after 200 000 voltage cycles (between 0.6 and 1.0 V/RHE at 50 mV $s^{-1}$).[136,166,167] The preparation of the Pt monolayer shell was performed by UPD of Cu followed by galvanic displacement of Pt (see route F in Figure 2). The improved durability was attributed to the increased stabilization of the very thin Pt shell in the form of a monolayer by the presence of Pd in the subsurface and the utilization of relatively large particles of 4−5 nm. Despite the increased stabilization of the Pt monolayer shell, a gradual dissolution of Pd from the subsurface was further observed after the durability test. Recently, potential-dependent structural memory effects in only Au−Pd nanoalloys have shown how dynamic surface processes of these more noble metals by changing the potential are affected and how the resulting catalytic properties are influenced.[120]

In another study, improved durability behavior and increased chemical stability were highlighted for Au/$Pt_3Fe$ core−shell nanoparticles.[168] The deposition of $Pt_3Fe$ on a pure Au particle core of 7 nm was prepared by organic solvothermal synthesis (see route E in Figure 2). The monodisperse core−shell nanoparticles consisting of a pure Au core and $Pt_3Fe$ shell with a final particle size of 10 nm were subjected to 60 000 voltage cycles (between 0.6 and 1.1 V/RHE at 50 mV $s^{-1}$). This study showed a drastically reduced loss of ECSA and ORR activity for this catalyst system. Activity benefits for the Au/$Pt_3Fe$ core−shell catalyst compared with those of the $Pt_3Fe$ alloy catalyst with a similar particle size of 10 nm were, however, not observed. It indicates no noticeable electronic/geometric influences of the existing Au core on the outermost Pt surface. Nevertheless, the resistance enhancement of the Au/$Pt_3Fe$ core−shell catalyst compared to the $Pt_3Fe$ alloy catalyst was attributed to the utilization of Au particle cores.

In summary, the lifetime and reactivity of core−shell nanocatalysts can be improved by careful tailoring of their structural and chemical properties like the Pt shell thickness, composition of the core, and particle size. Important degradation processes of core−shell nanoparticles seem to be Ostwald ripening, particle coalescence, shell thickness growth, and chemical instability of the particle core. Suppression of Pt redeposition and particle migration could be achieved by design of larger particles and by strengthening the interaction between the support material and catalytically active particles through, for example, heteroatoms. Despite recent progress, we are still lacking in a complete understanding of all of the various degradation and aging processes of core−shell nanoparticles over time. Precious metals as the particle core have shown improved stabilization of core−shell architectures; however, the corresponding benefits do not match the costs.

*Challenges and Perspectives.* Of all 170 years of fuel cell catalyst history, the past 15 years have seen an unprecedented explosion in our understanding and controlled design of highly active PEMFC electrocatalysts, in particular, for the sluggish kinetics of ORR. Recent catalyst designs and engineering have led to a manifold increase in the intrinsic ORR activity associated with a reduction of the amount of precious metal. Of those unique and versatile catalyst designs, Pt-based core−shell nanocatalysts have attracted special attention. At today's


dx.doi.org/10.1021/jz4014135 | J. Phys. Chem. Lett. 2013, 4, 3273−3291

development stage, Pt alloy core−shell nanoparticles appear to offer great potential to substitute pure Pt in PEM fuel cell applications in the near future.

Despite very intense research and development efforts in academia and industry over the past two decades, further improvements toward catalyst cost reduction and catalyst durability enhancement will remain an important challenge. To date, none of the discussed ORR electrocatalyst concepts has met, for technical and economic viability, the full stability targets in technological cells (~300 $cm^2$ active area) under realistic operating conditions.

The key for improving catalyst durability is principally to find a better understanding and a better level of control of the detailed parameters affecting degradation and catalyst stabilization. As indicated earlier, major degradation processes detrimental to the catalytic ORR performance of core−shell particles include (i) the continued depletion of metal atoms from the particle core, associated with the growth of the Pt-enriched shell, (ii) general particle growth and coarsening due to coalescence or Pt dissolution/redeposition, resulting in thicker Pt shell and complex intraparticle core structures, and (iii) the complete loss of the core−shell morphology due to the nanoporosity evolution or the formation of hollow particles. These three degradation processes strongly influence the synergic interaction of geometric surface lattice strain and electronic charge/ligand effects in the top atomic layers of Pt and lead to a gradual drop of catalytic activity over time. Therefore, to further improve catalyst stability and activity, a better understanding of these degradation processes and the associated changes in the atomic and electronic properties of the Pt-rich surface is necessary.

Current catalyst strategies to address the compositional stability of the particle core include the use of dopant atoms, for example, noble metal atoms or metal oxides in or near the surface of the particles. Particle migration and coarsening can be mitigated by stronger catalyst−support interaction or encapsulation of alloy nanoparticles in specifically tailored porous supports, where particle growth is limited by pore size. Moreover, the utilization of a carefully designed material support like heteroatom-doped carbons and oxide-based materials with a controlled hierarchical pore structure can help reduce particle growth and mobility. Moreover, ongoing research on dealloyed Pt core−shell nanoparticle catalysts has demonstrated that detrimental compositional changes, such as loss of the less noble alloy metal, and loss of core−shell morphology can be mitigated by carefully controlling the initial nanoparticle size distribution.[29] In fact, a carefully size-controlled dealloyed Pt−Ni nanoparticle catalyst has recently, for the first time, met and exceeded both the US DOE activity and the stability targets in 50 $cm^2$ single fuel cells under automotive conditions.[169]

Current and future strategies to further improve the catalytic activity of Pt alloy nanoparticles include the careful synthetic control of the nanoparticle shape, that is, the nature of the exposed facets, such as to expose only selected facets with the most favorable kinetics. However, control of the facet orientation alone is again not sufficient but requires additional control of the metal distribution among facet, edges, and corners, often a fairly difficult undertaking, as shown in Figure 9.[81]

Future developments of ever more powerful X-ray-based spectroscopic and scattering analytics as well as advanced in situ (environmental) microscopic characterization techniques will play a key role to fill our knowledge gap with regards to a complete atomic-scale understanding of degradation processes of core−shell nanoparticles. Theoretical and computational material science and electrocatalysis, including the combination of quantum chemical and Monte Carlo type predictions, will be indispensable in this context to better understand the relationship between microscopic materials parameters and chemical surface reactivity for advanced ORR core−shell catalysts. Altogether, the future of research on core−shell materials architectures is bright and holds the promise for further exciting insights and unexpected discoveries. Core−shell nanoparticles will clearly continue to be an important class of versatile functional materials for applications in catalysis and electrocatalysis such as fuel cells and electrolyzers.

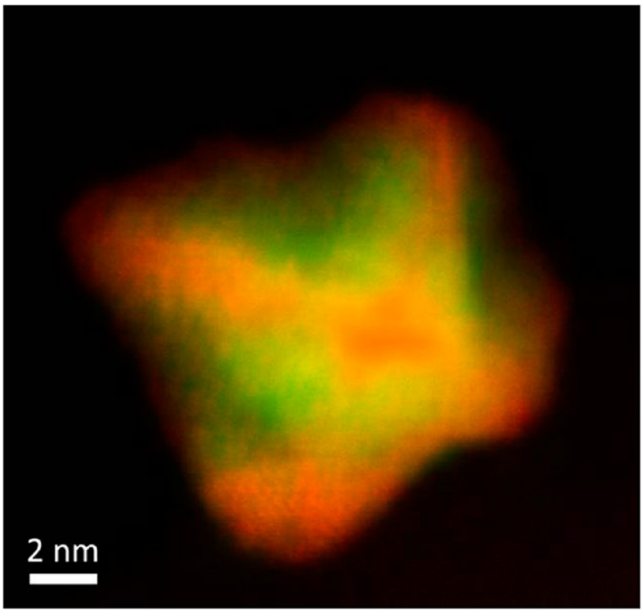


**Figure 9.** The Cs-corrected hybrid compositional map of as-prepared octahedral Pt−Ni nanoparticles demonstrates a complex surface distribution of dissimilar atoms across facets, corners, and edges. Reprinted from ref 81 with permission of Nature Publishing Group, copyright (2013).

Future developments of ever more powerful X-ray-based spectroscopic and scattering analytics as well as advanced in situ (environmental) microscopic characterization techniques will play a key role to fill our knowledge gap with regards to a complete atomic-scale understanding of degradation processes of core−shell nanoparticles.

## AUTHOR INFORMATION

### Corresponding Authors

*E-mail: mehtap.oezaslan@psi.ch (M.O.).
*E-mail: pstrasser@tu-berlin.de (P.S.).

## Present Address

[§]M.O.: The Electrochemistry Laboratory, Energy Research Department, Paul Scherrer Institut, 5232 Villigen, Switzerland.


## Notes

The authors declare no competing financial interest.

## Biographies

**Mehtap Oezaslan** is a scientist in the Electrochemistry Laboratory Group (Prof. Thomas J. Schmidt) at the Paul Scherrer Institut, Switzerland since 2012 (http://www.psi.ch/lec/electrocatalysis-and-interfaces). Her research is concerned with the development of electrocatalysts for PEM fuel cells and sustainable fuel production. She obtained her Dr. rer. nat. in electrochemistry from the Technische Universität Berlin in spring 2012.

Since 2012, **Frédéric Hasché** has been a postdoctoral fellow in Prof. Hubert A. Gasteiger's group at the Technische Universität München, Germany (http://www.tec.ch.tum.de). He is focused on PEM fuel cell diagnostics of single-cell membrane electrode assemblies as well as PEMFC stacks. He obtained his Dr. rer. nat. in electrochemistry from the Technische Universität Berlin in spring 2012.

**Peter Strasser** is a chaired full professor of Chemical Engineering at the Technische Universität Berlin (http://www.technischechemie.tu-berlin.de). He was Assistant Professor at the University of Houston and, before that, held a senior research position at Symyx Technologies. He obtained his Ph.D. in physical chemistry and electrochemistry under Gerhard Ertl at the Fritz-Haber Institute of the Max-Planck Society, Berlin.

## REFERENCES


(1) Gasteiger, H.; Baker, D. R.; Carter, R. N.; Gu, W.; Liu, Y.; Wagner, F. T.; Yu, P. T. In *Hydrogen Fuel Cells: Fundamentals, Technologies and Applications* ; Stolten, D., Ed.; Wiley-VCH: Weinheim, Germany, 2010.

(2) Gasteiger, H. A.; Kocha, S. S.; Sompalli, B.; Wagner, F. T. Activity Benchmarks and Requirements for Pt, Pt−Alloy, and Non-Pt Oxygen Reduction Catalysts for PEMFCs. *Appl. Catal., B* **2005**, *56*, 9−35.

(3) Hwang, S. J.; Yoo, S. J.; Shin, J.; Cho, Y.-H.; Jang, J. H.; Cho, E.; Sung, Y.-E.; Nam, S. W.; Lim, T.-H.; Lee, S.-C.; et al. Supported Core@Shell Electrocatalysts for Fuel Cells: Close Encounter with Reality. *Sci. Rep.* **2013**, *3*, 1−7.

(4) Neyerlin, K. C.; Gu, W. B.; Jorne, J.; Gasteiger, H. A. Study of the Exchange Current Density for the Hydrogen Oxidation and Evolution Reactions. *J. Electrochem. Soc.* **2007**, *154*, B631−B635.

(5) Department of Energy. *Table 3.4.13 Technical Targets: Electrocatalysts for Transportation Applications*. http://www.eere.energy.gov (2011).

(6) Department of Energy. *Doe Cell Component Accelerated Stress Test Protocols for PEM Fuel Cells*; March 2007.

(7) Japanese New Energy and Industrial Technology Development Organization (NEDO). http://www.nedo.go.jp/english/index.html (June 2013).

(8) Fuel Cells and Hydrogen Joint Undertaking, European Commission. http://www.fch-ju.eu (June 2013).

(9) Rabis, A.; Rodriguez, P.; Schmidt, T. J. Electrocatalysis for Polymer Electrolyte Fuel Cells: Recent Achievements and Future Challenges. *ACS Catal.* **2012**, *2*, 864−890.

(10) Chorkendorff, I.; Stephens, I. E. L.; Bondarenko, A. S.; Andersen, U. G.; Rossmeisl, J. Understanding the Electrocatalysis of Oxygen Reduction on Platinum and Its Alloys. *Energy Environ. Sci.* **2012**, *5*, 6744−6762.

(11) Debe, M. K. Electrocatalyst Approaches and Challenges for Automotive Fuel Cells. *Nature* **2012**, *486*, 43−51.

(12) Swider-Lyons, K. E.; Campbell, S. A. Physical Chemistry Research Toward Proton Exchange Membrane Fuel Cell Advancement. *J. Phys. Chem. Lett.* **2013**, *4*, 393−401.

(13) Anderson, A. B.; Roque, J.; Mukerjee, S.; Murthi, V. S.; Markovic, N. M.; Stamenkovic, V. Activation Energies for Oxygen Reduction on Platinum Alloys: Theory and Experiment. *J. Phys. Chem. B* **2005**, *109*, 1198−1203.

(14) Anderson, A. Volcano Plots and Effective Reversible Potentials for Oxygen Electroreduction. *Electrocatalysis* **2012**, *3*, 1−7.

(15) Greeley, J.; Stephens, I. E. L.; Bondarenko, A. S.; Johansson, T. P.; Hansen, H. A.; Jaramillo, T. F.; Rossmeisl, J.; Chorkendorff, I.; Norskov, J. K. Alloys of Platinum and Early Transition Metals As Oxygen Reduction Electrocatalysts. *Nat. Chem.* **2009**, *1*, 552−556.

(16) Hammer, B.; Norskov, J. K. Theoretical Surface Science and Catalysis — Calculations and Concepts. *Adv. Catal.* **2000**, *45*, 71−129.

(17) Norskov, J. K.; Rossmeisl, J.; Logadottir, A.; Lindqvist, L.; Kitchin, J. R.; Bligaard, T.; Jonsson, H. Origin of the Overpotential for Oxygen Reduction at a Fuel-Cell Cathode. *J. Phys. Chem. B* **2004**, *108*, 17886−17892.

(18) Bligaard, T.; Norskov, J. K.; Dahl, S.; Matthiesen, J.; Christensen, C. H.; Sehested, J. The Brønsted−Evans−Polanyi Relation and the Volcano Curve in Heterogeneous Catalysis. *J. Catal.* **2004**, *224*, 206−217.

(19) Debe, M. K.; Schmoeckel, A. K.; Vernstrom, G. D.; Atanasoski, R. High Voltage Stability of Nanostructured Thin Film Catalysts for PEM Fuel Cells. *J. Power Sources* **2006**, *161*, 1002−1011.

(20) Stonehart, P. Development of Advanced Noble Metal−Alloy Electrocatalysts for Phosphoric Acid Fuel Cells (PAFC). *Ber. Bunsen-Ges. Phys. Chem.* **1990**, *94*, 913−921.

(21) Stonehart, P. Development of Alloy Electrocatalysts for Phosphoric Acid Fuel Cells (PAFC). *J. Appl. Electrochem.* **1992**, *22*, 995−1001.

(22) Luczak, F. J.; Landsman, D. A. *Ternary Fuel Cell Catalysts Containing Platinum, Cobalt and Cromium*. U.S. Patent 4,447,506, 1984.

(23) Toda, T.; Igarashi, H.; Watanabe, M. Role of Electronic Property of Pt and Pt Alloys on Electrocatalytic Reduction of Oxygen. *J. Electrochem. Soc.* **1998**, *145*, 4185−4188.

(24) Toda, T.; Igarashi, H.; Uchida, H.; Watanabe, M. Enhancement of the Electroreduction of Oxygen on Pt Alloys with Fe, Ni, and Co. *J. Electrochem. Soc.* **1999**, *146*, 3750−3756.

(25) Oezaslan, M.; Strasser, P. Activity of Dealloyed $PtCo_3$ and $PtCu_3$ Nanoparticle Electrocatalyst for Oxygen Reduction Reaction in Polymer Electrolyte Membrane Fuel Cell. *J. Power Sources* **2011**, *196*, 5240−5249.

(26) Oezaslan, M.; Hasché, F.; Strasser, P. Oxygen Electroreduction on $PtCo_3$, PtCo and $Pt_3Co$ Alloy Nanoparticles for Alkaline and Acidic PEM Fuel Cells. *J. Electrochem. Soc.* **2012**, *159*, B394−B405.

(27) Oezaslan, M.; Hasché, F.; Strasser, P. $PtCu_3$, PtCu and $Pt_3Cu$ Alloy Nanoparticle Electrocatalysts for Oxygen Reduction Reaction in Alkaline and Acidic Media. *J. Electrochem. Soc.* **2012**, *159*, B444−B454.

(28) Hasché, F.; Oezaslan, M.; Strasser, P. Activity, Structure and Degradation of Dealloyed $PtNi_3$ Nanoparticle Electrocatalyst for the Oxygen Reduction Reaction in PEMFC. *J. Electrochem. Soc.* **2012**, *159*, B25−B34.

(29) Gan, L.; Heggen, M.; O'Malley, R.; Theobald, B.; Strasser, P. Understanding and Controlling Nanoporosity Formation for Improving the Stability of Bimetallic Fuel Cell Catalysts. *Nano Lett.* **2013**, *13*, 1131−1138.

(30) Rudi, S.; Tuaev, X.; Strasser, P. Electrocatalytic Oxygen Reduction on Dealloyed $Pt_{1-x}Ni_x$ Alloy Nanoparticle Electrocatalysts. *Electrocatalysis* **2012**, *3*, 265−273.

(31) Gan, L.; Heggen, M.; Rudi, S.; Strasser, P. Core−Shell Compositional Fine Structures of Dealloyed $Pt_xNi_{1-x}$ Nanoparticles and Their Impact on Oxygen Reduction Catalysis. *Nano Lett.* **2012**, *12*, 5423−5430.

(32) Cui, C.; Gan, L.; Li, H.-H.; Yu, S.-H.; Heggen, M.; Strasser, P. Octahedral PtNi Nanoparticle Catalysts: Exceptional Oxygen Reduction Activity by Tuning the Alloy Particle Surface Composition. *Nano Lett.* **2012**, *12*, 5885−5889.

(33) Kitchin, J. R.; Norskov, J. K.; Barteau, M. A.; Chen, J. G. Modification of the Surface Electronic and Chemical Properties of

Pt(111) by Subsurface 3 d Transition Metals. *J. Chem. Phys.* **2004**, *120*, 10240−10246.
(34) Kitchin, J. R.; Norskov, J. K.; Barteau, M. A.; Chen, J. G. Role of Strain and Ligand Effects in the Modification of the Electronic and Chemical Properties of Bimetallic Surfaces. *Phys. Rev. Lett.* **2004**, *93*, 156801.
(35) Strasser, P.; Koh, S.; Anniyev, T.; Greeley, J.; More, K.; Yu, C.; Liu, Z.; Kaya, S.; Nordlund, D.; Ogasawara, H.; et al. Lattice-Strain Control of the Activity in Dealloyed Core−Shell Fuel Cell Catalysts. *Nat. Chem.* **2010**, *2*, 454−460.
(36) Yu, C.; Koh, S.; Leisch, J. E.; Toney, M. F.; Strasser, P. Size and Composition Distribution Dynamics of Alloy Nanoparticle Electrocatalysts Probed by Anomalous Small Angle X-ray Scattering (ASAXS). *Faraday Discuss.* **2009**, *140*, 283−296.
(37) Yang, H. Platinum-Based Electrocatalysts with Core−Shell Nanostructures. *Angew. Chem., Int. Ed.* **2011**, *50*, 2674−2676.
(38) Bezerra, C. W. B.; Zhang, L.; Liu, H.; Lee, K.; Marques, A. L. B.; Marques, E. P.; Wang, H.; Zhang, J. A Review of Heat-Treatment Effects on Activity and Stability of PEM Fuel Cell Catalysts for Oxygen Reduction Reaction. *J. Power Sources* **2007**, *173*, 891−908.
(39) Borup, R.; Meyers, J.; Pivovar, B.; Kim, Y. S.; Mukundan, R.; Garland, N.; Myers, D.; Wilson, M.; Garzon, F.; Wood, D.; et al. Scientific Aspects of Polymer Electrolyte Fuel Cell Durability and Degradation. *Chem. Rev.* **2007**, *107*, 3904−3951.
(40) Jaouen, F.; Herranz, J.; Lefevre, M.; Dodelet, J.-P.; Kramm, U. I.; Herrmann, I.; Bogdanoff, P.; Maruyama, J.; Nagaoka, T.; Garsuch, A.; et al. Cross-Laboratory Experimental Study of Non-Noble-Metal Electrocatalysts for the Oxygen Reduction Reaction. *ACS Appl. Mater. Interfaces* **2009**, *1*, 1623−1639.
(41) Koenigsmann, C.; Scofield, M. E.; Liu, H.; Wong, S. S. Designing Enhanced One-Dimensional Electrocatalysts for the Oxygen Reduction Reaction: Probing Size- and Composition-Dependent Electrocatalytic Behavior in Noble Metal Nanowires. *J. Phys. Chem. Lett.* **2012**, *3*, 3385−3398.
(42) Xia, B. Y.; Wu, H. B.; Yan, Y.; Lou, X. W.; Wang, X. Ultrathin and Ultralong Single-Crystal Platinum Nanowire Assemblies with Highly Stable Electrocatalytic Activity. *J. Am. Chem. Soc.* **2013**, *135*, 9480−9485.
(43) Ramirez-Caballero, G. E.; Ma, Y.; Callejas-Tovar, R.; Balbuena, P. B. Surface Segregation and Stability of Core−Shell Alloy Catalysts for Oxygen Reduction in Acid Medium. *Phys. Chem. Chem. Phys.* **2010**, *12*, 2209−2218.
(44) Ramirez-Caballero, G. E.; Balbuena, P. B. Surface Segregation of Core Atoms in Core−Shell Structures. *Chem. Phys. Lett.* **2008**, *456*, 64−67.
(45) Ramírez-Caballero, G. E.; Balbuena, P. B. Dissolution-Resistant Core−Shell Materials for Acid Medium Oxygen Reduction Electrocatalysts. *J. Phys. Chem. Lett.* **2010**, *1*, 724−728.
(46) Esposito, D. V.; Hunt, S. T.; Kimmel, Y. C.; Chen, J. G. A New Class of Electrocatalysts for Hydrogen Production from Water Electrolysis: Metal Monolayers Supported on Low-Cost Transition Metal Carbides. *J. Am. Chem. Soc.* **2012**, *134*, 3025−3033.
(47) Esposito, D. V.; Hunt, S. T.; Stottlemyer, A. L.; Dobson, K. D.; McCandless, B. E.; Birkmire, R. W.; Chen, J. G. Low-Cost Hydrogen-Evolution Catalysts Based on Monolayer Platinum on Tungsten Monocarbide Substrates. *Angew. Chem., Int. Ed.* **2010**, *49*, 9859−9862.
(48) Stephens, I. E. L.; Bondarenko, A. S.; Bech, L.; Chorkendorff, I. Oxygen Electroreduction Activity and X-ray Photoelectron Spectroscopy of Platinum and Early Transition Metal Alloys. *ChemCatChem* **2012**, *4*, 341−349.
(49) Escudero-Escribano, M.; Verdaguer-Casadevall, A.; Malacrida, P.; Grønbjerg, U.; Knudsen, B. P.; Jepsen, A. K.; Rossmeisl, J.; Stephens, I. E. L.; Chorkendorff, I. $Pt_5Gd$ as a Highly Active and Stable Catalyst for Oxygen Electroreduction. *J. Am. Chem. Soc.* **2012**, *134*, 16476−16479.
(50) Kinoshita, K. Particle Size Effects for Oxygen Reduction on Highly Dispersed Platinum in Acid Electrolytes. *J. Electrochem. Soc.* **1990**, *137*, 845−848.
(51) Nesselberger, M.; Ashton, S.; Meier, J. C.; Katsounaros, I.; Mayrhofer, K. J. J.; Arenz, M. The Particle Size Effect on the Oxygen Reduction Reaction Activity of Pt Catalysts: Influence of Electrolyte and Relation to Single Crystal Models. *J. Am. Chem. Soc.* **2011**, *133*, 17428−17433.
(52) Mayrhofer, K. J. J.; Blizanac, B. B.; Arenz, M.; Stamenkovic, V. R.; Ross, P. N.; Markovic, N. M. The Impact of Geometric and Surface Electronic Properties of Pt-Catalysts on the Particle Size Effect in Electrocatalysis. *J. Phys. Chem. B* **2005**, *109*, 14433−14440.
(53) Watanabe, M.; Sei, H.; Stonehart, P. The Influence of Platinum Crystallite Size on the Electroreduction of Oxygen. *J. Electroanal. Chem.* **1989**, *261*, 375−387.
(54) Perez-Alonso, F. J.; McCarthy, D. N.; Nierhoff, A.; Hernandez-Fernandez, P.; Strebel, C.; Stephens, I. E. L.; Nielsen, J. H.; Chorkendorff, I. The Effect of Size on the Oxygen Electroreduction Activity of Mass-Selected Platinum Nanoparticles. *Angew. Chem., Int. Ed.* **2012**, *51*, 4641−4643.
(55) Shao-Horn, Y.; Sheng, W.; Chen, S.; Ferreira, P.; Holby, E.; Morgan, D. Instability of Supported Platinum Nanoparticles in Low-Temperature Fuel Cells. *Top. Catal.* **2007**, *46*, 285−305.
(56) Holby, E. F.; Sheng, W.; Shao-Horn, Y.; Morgan, D. Pt Nanoparticle Stability in PEM Fuel Cells: Influence of Particle Size Distribution and Crossover Hydrogen. *Energy Environ. Sci.* **2009**, *2*, 865−871.
(57) Ferreira, P. J.; la O', G. J.; Shao-Horn, Y.; Morgan, D.; Makharia, R.; Kocha, S.; Gasteiger, H. A. Instability of Pt/C Electrocatalysts in Proton Exchange Membrane Fuel Cells. *J. Electrochem. Soc.* **2005**, *152*, A2256−A2271.
(58) Hasché, F.; Oezaslan, M.; Strasser, P. Activity, Stability and Degradation of Multi Walled Carbon Nanotube (MWCNT) Supported Pt Fuel Cell Electrocatalysts. *Phys. Chem. Chem. Phys.* **2010**, *12*, 15251−15258.
(59) Hasché, F.; Oezaslan, M.; Strasser, P. Activity, Stability, and Degradation Mechanisms of Dealloyed $PtCu_3$ and $PtCo_3$ Nanoparticle Fuel Cell Catalysts. *ChemCatChem* **2011**, *3*, 1805−1813.
(60) Hasché, F.; Oezaslan, M.; Strasser, P. In Situ Observation of Thermal Induced Growth of Platinum Nanoparticle Catalyst Using High Temperature X-ray Diffraction. *ChemPhysChem* **2012**, *13*, 828−834.
(61) Hasché, F.; Fellinger, T.-P.; Oezaslan, M.; Paraknowitsch, J. P.; Antonietti, M.; Strasser, P. Mesoporous Nitrogen Doped Carbon Supported Platinum PEM Fuel Cell Electrocatalyst Made from Ionic Liquids. *ChemCatChem* **2012**, *4*, 479−483.
(62) Tang, L.; Li, X.; Cammarata, R. C.; Friesen, C.; Sieradzki, K. Electrochemical Stability of Elemental Metal Nanoparticles. *J. Am. Chem. Soc.* **2010**, *132*, 11722−11726.
(63) Erlebacher, J. Mechanism of Coarsening and Bubble Formation in High-Genus Nanoporous Metals. *Phys. Rev. Lett.* **2011**, *106*, 225504.
(64) Erlebacher, J.; Aziz, M. J.; Karma, A.; Dimitrov, N.; Sieradzki, K. Evolution of Nanoporosity in Dealloying. *Nature* **2001**, *410*, 450−453.
(65) Oezaslan, M.; Heggen, M.; Strasser, P. Size-Dependent Morphology of Dealloyed Bimetallic Catalysts: Linking the Nano to the Macro Scale. *J. Am. Chem. Soc.* **2012**, *134*, 514−524.
(66) Oezaslan, M.; Heggen, M.; Hasché, F.; Strasser, P. Core−Shell Fine Structure and Size-Dependent Morphology of Dealloyed Pt Bimetallic Nanoparticle Fuel Cell Electrocatalysts. *ECS Trans.* **2013**, *50*, 1633−1641.
(67) Markovic, N.; Gasteiger, H.; Ross, P. N. Kinetics of Oxygen Reduction on Pt(hkl) Electrodes: Implications for the Crystallite Size Effect with Supported Pt Electrocatalysts. *J. Electrochem. Soc.* **1997**, *144*, 1591−1597.
(68) Schmidt, T. J.; Stamenkovic, V.; Ross, P. N., Jr.; Markovic, N. M. Temperature Dependent Surface Electrochemistry on Pt Single Crystals in Alkaline Electrolyte. *Phys. Chem. Chem. Phys.* **2003**, *5*, 400−406.
(69) Markovic, N. M.; Gasteiger, H. A.; Ross, P. N., Jr. Oxygen Reduction on Platinum Low-Index Single-Crystal Surfaces in Sulfuric Acid Solution: Rotating Ring-Pt(hkl) Disk Studies. *J. Phys. Chem.* **1995**, *99*, 3411−3415.

(70) Stamenkovic, V.; Moon, B. S.; Mayerhofer, K. J.; Ross, P. N.; Markovic, N.; Rossmeisl, J.; Greeley, J.; Norskov, J. K. Changing the Activity of Electrocatalysts for Oxygen Reduction by Tuning the Surface Electronic Structure. *Angew. Chem., Int. Ed.* **2006**, *45*, 2897−2901.
(71) Stamenkovic, V. R.; Fowler, B.; Mun, B. S.; Wang, G.; Ross, P. N.; Lucas, C. A.; Markovic, N. M. Improved Oxygen Reduction Activity on $Pt_3Ni(111)$ via Increased Surface Site Availability. *Science* **2007**, *315*, 493−497.
(72) Stamenkovic, V. R.; Mun, B. S.; Mayrhofer, K. J. J.; Ross, P. N.; Markovic, N. M. Effect of Surface Composition on Electronic Structure, Stability, and Electrocatalytic Properties of Pt-Transition Metal Alloys: Pt-Skin versus Pt-Skeleton Surfaces. *J. Am. Chem. Soc.* **2006**, *128*, 8702−8988.
(73) Stamenkovic, V. R.; Mun, B. S.; Arenz, M.; Mayrhofer, K. J. J.; Lucas, C. A.; Wang, G.; Ross, P. N.; Markovic, N. M. Trends in Electrocatalysis on Extended and Nanoscale Pt−Bimetallic Alloy Surfaces. *Nat. Mater.* **2007**, *6*, 241−247.
(74) Markovic, N. M.; Gasteiger, H. A.; Ross, P. N. Oxygen Reduction on Platinum Low-Index Single-Crystal Surfaces in Alkaline Solution: Rotating Ring Disk Pt(hkl) Studies. *J. Phys. Chem.* **1996**, *100*, 6715−6721.
(75) Stamenkovic, V. R.; Fowler, B.; Mun, B. S.; Wang, G. F.; Ross, P. N.; Lucas, C. A.; Markovic, N. M. Improved Oxygen Reduction Activity on $Pt_3Ni(111)$ via Increased Surface Site Availability. *Science* **2007**, *315*, 493−497.
(76) Gu, J.; Zhang, Y. W.; Tao, F. Shape Control of Bimetallic Nanocatalysts through Well-Designed Colloidal Chemistry Approaches. *Chem. Soc. Rev.* **2012**, *41*, 8050−8065.
(77) Wu, J.; Zhang, J.; Peng, Z.; Yang, S.; Wagner, F. T.; Yang, H. Truncated Octahedral $Pt_3Ni$ Oxygen Reduction Reaction Electrocatalysts. *J. Am. Chem. Soc.* **2010**, *132*, 4984−4985.
(78) Wu, J. B.; Gross, A.; Yang, H. Shape and Composition-Controlled Platinum Alloy Nanocrystals Using Carbon Monoxide as Reducing Agent. *Nano Lett.* **2011**, *11*, 798−802.
(79) Zhang, J.; Yang, H.; Fang, J.; Zou, S. Synthesis and Oxygen Reduction Activity of Shape-Controlled $Pt_3Ni$ Nanopolyhedra. *Nano Lett.* **2010**, *10*, 638.
(80) Carpenter, M. K.; Moylan, T. E.; Kukreja, R. S.; Atwan, M. H.; Tessema, M. M. Solvothermal Synthesis of Platinum Alloy Nanoparticles for Oxygen Reduction Electrocatalysis. *J. Am. Chem. Soc.* **2012**, *134*, 8535−8542.
(81) Cui, C.; Gan, L.; Heggen, M.; Rudi, S.; Strasser, P. Compositional Segregation in Shaped Pt Alloy Nanoparticles and Their Structural Behaviour during Electrocatalysis. *Nat. Mater.* **2013**, 1−7.
(82) Wu, Y.; Wang, D.; Niu, Z.; Chen, P.; Zhou, G.; Li, Y. A Strategy for Designing a Concave Pt−Ni Alloy through Controllable Chemical Etching. *Angew. Chem., Int. Ed.* **2012**, *51*, 12524−12528.
(83) Yang, R.; Leisch, J.; Strasser, P.; Toney, M. F. Structure of Dealloyed $PtCu_3$ Thin Films and Catalytic Activity for Oxygen Reduction. *Chem. Mater.* **2010**, *22*, 4712−4720.
(84) Yang, R.; Strasser, P.; Toney, M. F. Dealloying of $Cu_3Pt$ (111) Studied by Surface X-ray Scattering. *J. Phys. Chem. C* **2011**, *115*, 9074−9080.
(85) Liu, Y.; Hangarter, C. M.; Bertocci, U.; Moffat, T. P. Oxygen Reduction Reaction on Electrodeposited $Pt_{100-x}Ni_x$: Influence of Alloy Composition and Dealloying. *J. Phys. Chem. C* **2012**, *116*, 7848−7862.
(86) Renner, F. U.; Stierle, A.; Dosch, H.; Kolb, D. M.; Lee, T. L.; Zegenhagen, J. In Situ X-ray Diffraction Study of the Initial Dealloying and Passivation of $Cu_3Au(111)$ during Anodic Dissolution. *Phys. Rev. B* **2008**, *77*, 235433.
(87) Renner, F. U.; Stierle, A.; Dosch, H.; Kolb, D. M.; Lee, T. L.; Zegenhagen, J. Initial Corrosion Observed on the Atomic Scale. *Nature* **2006**, *439*, 707−710.
(88) Borchert, H.; Shevchenko, E. V.; Robert, A.; Mekis, I.; Kornowski, A.; Grübel, G.; Weller, H. Determination of Nanocrystal Sizes: A Comparison of TEM, SAXS, and XRD Studies of Highly Monodisperse $CoPt_3$ Particles. *Langmuir* **2005**, *21*, 1931−1936.
(89) Yang, R.; Bian, W.; Strasser, P.; Toney, M. F. Dealloyed $PdCu_3$ Thin Film Electrocatalysts for Oxygen Reduction Reaction. *J. Power Sources* **2013**, *222*, 169−176.
(90) Koh, S.; Strasser, P. Electrocatalysis on Bimetallic Surfaces: Modifying Catalytic Reactivity for Oxygen Reduction by Voltammetric Surface Dealloying. *J. Am. Chem. Soc.* **2007**, *129*, 12624−12625.
(91) Srivastava, R.; Mani, P.; Hahn, N.; Strasser, P. Efficient Oxygen Reduction Fuel Cell Electrocatalysis on Voltammetrically Dealloyed Pt−Cu−Co Nanoparticles. *Angew. Chem., Int. Ed.* **2007**, *46*, 8988−8991.
(92) Oezaslan, M.; Hasché, F.; Strasser, P. In-Situ High Temperature X-ray Diffraction Study of $PtCu_3$ Alloy Electrocatalyst for PEMFC. *Z. Anorg. Allg. Chem.* **2010**, *636*, 2111−2111.
(93) Oezaslan, M.; Hasché, F.; Strasser, P. In Situ Observation of Bimetallic Alloy Nanoparticle Formation and Growth Using High-Temperature XRD. *Chem. Mater.* **2011**, *23*, 2159−2165.
(94) Wang, C.; van der Vliet, D.; Chang, K.-C.; You, H.; Strmcnik, D.; Schlueter, J. A.; Markovic, N. M.; Stamenkovic, V. R. Monodisperse $Pt_3Co$ Nanoparticles as a Catalyst for the Oxygen Reduction Reaction: Size-Dependent Activity. *J. Phys. Chem. C* **2009**, *113*, 19365−19368.
(95) Wang, C.; Chi, M.; Wang, G.; van der Vliet, D.; Li, D.; More, K.; Wang, H.-H.; Schlueter, J. A.; Markovic, N. M.; Stamenkovic, V. R. Correlation Between Surface Chemistry and Electrocatalytic Properties of Monodisperse $Pt_xNi_{1-x}$ Nanoparticles. *Adv. Funct. Mater.* **2011**, *21*, 147−152.
(96) Wang, C.; Wang, G.; van der Vliet, D.; Chang, K.-C.; Markovic, N. M.; Stamenkovic, V. R. Monodisperse $Pt_3Co$ Nanoparticles As Electrocatalyst: The Effects of Particle Size and Pretreatment on Electrocatalytic Reduction of Oxygen. *Phys. Chem. Chem. Phys.* **2010**, *12*, 6933−6939.
(97) Snyder, J.; McCue, I.; Livi, K. J.; Erlebacher, J. D. Structure/Processing/Properties Relationships in Nanoporous Nanoparticles as Applied to Catalysis of the Cathodic Oxygen Reduction Reaction. *J. Am. Chem. Soc.* **2012**, *134*, 8633−8645.
(98) Finney, E. E.; Finke, R. G. Nanocluster Nucleation and Growth Kinetic and Mechanistic Studies: A Review Emphasizing Transition-Metal Nanoclusters. *J. Colloid Interface Sci.* **2008**, *317*, 351−374.
(99) LaMer, V. K.; Dinegar, R. H. Theory, Production and Mechanism of Formation of Monodispersed Hydrosols. *J. Am. Chem. Soc.* **1950**, *72*, 4847−4854.
(100) Gan, L.; Yu, R.; Luo, J.; Cheng, Z.; Zhu, J. Lattice Strain Distributions in Individual Dealloyed Pt−Fe Catalyst Nanoparticles. *J. Phys. Chem. Lett.* **2012**, *3*, 934−938.
(101) Chen, S.; Gasteiger, H. A.; Hayakawa, K.; Tada, T.; Shao-Horn, Y. Platinum-Alloy Cathode Catalyst Degradation in Proton Exchange Membrane Fuel Cells: Nanometer-Scale Compositional and Morphological Changes. *J. Electrochem. Soc.* **2010**, *157*, A82−A97.
(102) Andersson, K. J.; Calle-Vallejo, F.; Rossmeisl, J.; Chorkendorff, I. Adsorption-Driven Surface Segregation of the Less Reactive Alloy Component. *J. Am. Chem. Soc.* **2009**, *131*, 2404−2407.
(103) Tao, F.; Grass, M. E.; Zhang, Y.; Butcher, D. R.; Renzas, J. R.; Liu, Z.; Chung, J. Y.; Mun, B. S.; Salmeron, M.; Somorjai, G. A. Reaction-Driven Restructuring of Rh−Pd and Pt−Pd Core−Shell Nanoparticles. *Science* **2008**, *322*, 932−934.
(104) Mayrhofer, K. J. J.; Juhart, V.; Hartl, K.; Hanzlik, M.; Arenz, M. Adsorbate-Induced Surface Segregation for Core−Shell Nanocatalysts. *Angew. Chem., Int. Ed.* **2009**, *48*, 3529−3531.
(105) Christensen, A.; Ruban, A. V.; Stoltze, P.; Jacobsen, K. W.; Skriver, H. L.; Nørskov, J. K.; Besenbacher, F. Phase Diagrams for Surface Alloys. *Phys. Rev. B* **1997**, *56*, 5822−5834.
(106) Lee, M. H.; Do, J. S. Kinetics of Oxygen Reduction Reaction on $Co_{rich\ core}$−$Pt_{rich\ shell}$/C Electrocatalysts. *J. Power Sources* **2009**, *188*, 353−358.
(107) Wang, C.; van der Vliet, D.; More, K. L.; Zaluzec, N. J.; Peng, S.; Sun, S.; Daimon, H.; Wang, G.; Greeley, J.; Pearson, J.; et al. Multimetallic Au/$FePt_3$ Nanoparticles as Highly Durable Electrocatalyst. *Nano Lett.* **2011**, *11*, 919−926.

(108) Zhao, D.; Xu, B.-Q. Enhancement of Pt Utilization in Electrocatalysts by Using Gold Nanoparticles. *Angew. Chem., Int. Ed.* **2006**, *45*, 4955−4959.
(109) Zhao, D.; Xu, B.-Q. Platinum Covering of Gold Nanoparticles for Utilization Enhancement of Pt in Electrocatalysts. *Phys. Chem. Chem. Phys.* **2006**, *8*, 5106−5114.
(110) Wang, Y.; Toshima, N. Preparation of Pd−Pt Bimetallic Colloids with Controllable Core/Shell Structures. *J. Phys. Chem. B* **1997**, *101*, 5301−5306.
(111) Zhou, S.; Varughese, B.; Eichhorn, B.; Jackson, G.; McIlwrath, K. Pt−Cu Core−Shell and Alloy Nanoparticles for Heterogeneous $NO_x$ Reduction: Anomalous Stability and Reactivity of a Core−Shell Nanostructure. *Angew. Chem., Int. Ed.* **2005**, *44*, 4539−4543.
(112) Teng, X.; Black, D.; Watkins, N. J.; Gao, Y.; Yang, H. Platinum−Maghemite Core−Shell Nanoparticles Using a Sequential Synthesis. *Nano Lett.* **2003**, *3*, 261−264.
(113) Peng, Z.; Yang, H. Designer Platinum Nanoparticles: Control of Shape, Composition in Alloy, Nanostructure and Electrocatalytic Property. *Nano Today* **2009**, *4*, 143−164.
(114) Campbell, C. T.; Sellers, J. R. V. Anchored Metal Nanoparticles: Effects of Support and Size on Their Energy, Sintering Resistance and Reactivity. *Faraday Discuss.* **2013**, *162*, 9−30.
(115) Chambers, S. A. Epitaxial Growth and Properties of Thin Film Oxides. *Surf. Sci. Rep.* **2000**, *39*, 105−180.
(116) Campbell, C. T.; Parker, S. C.; Starr, D. E. The Effect of Size-Dependent Nanoparticle Energetics on Catalyst Sintering. *Science* **2002**, *298*, 811−814.
(117) Wang, J. X.; Inada, H.; Wu, L.; Zhu, Y.; Choi, Y.; Liu, P.; Zhou, W.-P.; Adzic, R. R. Oxygen Reduction on Well-Defined Core−Shell Nanocatalysts: Particle Size, Facet, and Pt Shell Thickness Effects. *J. Am. Chem. Soc.* **2009**, *131*, 17298−17302.
(118) Zhang, J.; Mo, Y.; Vukmirovic, M.; Klie, R.; Sasaki, K.; Adzic, R. Platinum Monolayer Electrocatalysts for $O_2$ Reduction: Pt Monolayer on Pd (111) and on Carbon-Supported Pd Nanoparticles. *J. Phys. Chem. B* **2004**, *108*, 10955−10964.
(119) Zhang, J. L.; Vukmirovic, M. B.; Sasaki, K.; Nilekar, A. U.; Mavrikakis, M.; Adzic, R. R. Mixed-Metal Pt Monolayer Electrocatalysts for Enhanced Oxygen Reduction Kinetics. *J. Am. Chem. Soc.* **2005**, *127*, 12480−12481.
(120) Sasaki, K.; Naohara, H.; Cai, Y.; Choi, Y. M.; Liu, P.; Vukmirovic, M. B.; Wang, J. X.; Adzic, R. R. Core-Protected Platinum Monolayer Shell High-Stability Electrocatalysts for Fuel-Cell Cathodes. *Angew. Chem., Int. Ed.* **2010**, *49*, 8602−8607.
(121) Karan, H. I.; Sasaki, K.; Kuttiyiel, K.; Farberow, C. A.; Mavrikakis, M.; Adzic, R. R. Catalytic Activity of Platinum Monolayer on Iridium and Rhenium Alloy Nanoparticles for the Oxygen Reduction Reaction. *ACS Catal.* **2012**, *2*, 817−824.
(122) Xing, Y.; Cai, Y.; Vukmirovic, M. B.; Zhou, W.-P.; Karan, H.; Wang, J. X.; Adzic, R. R. Enhancing Oxygen Reduction Reaction Activity via Pd−Au Alloy Sublayer Mediation of Pt Monolayer Electrocatalysts. *J. Phys. Chem. Lett.* **2010**, *1*, 3238−3242.
(123) Li, M.; Liu, P.; Adzic, R. R. Platinum Monolayer Electrocatalysts for Anodic Oxidation of Alcohols. *J. Phys. Chem. Lett.* **2012**, *3*, 3480−3485.
(124) Shao, M.; Peles, A.; Shoemaker, K.; Gummalla, M.; Njoki, P. N.; Luo, J.; Zhong, C.-J. Enhanced Oxygen Reduction Activity of Platinum Monolayer on Gold Nanoparticles. *J. Phys. Chem. Lett.* **2010**, *2*, 67−72.
(125) Sarkar, A.; Manthiram, A. Synthesis of Pt@Cu Core−Shell Nanoparticles by Galvanic Displacement of Cu by $Pt^{4+}$ Ions and Their Application as Electrocatalysts for Oxygen Reduction Reaction in Fuel Cells. *J. Phys. Chem. C* **2010**, *114*, 4725−4732.
(126) Cochell, T.; Manthiram, A. Pt@$Pd_xCu_y$/C Core−Shell Electrocatalysts for Oxygen Reduction Reaction in Fuel Cells. *Langmuir* **2011**, *28*, 1579−1587.
(127) Tenney, S.; He, W.; Ratliff, J.; Mullins, D.; Chen, D. Characterization of Pt−Au and Ni−Au Clusters on $TiO_2$(110). *Top. Catal.* **2011**, *54*, 42−55.
(128) Tenney, S. A.; He, W.; Roberts, C. C.; Ratliff, J. S.; Shah, S. I.; Shafai, G. S.; Turkowski, V.; Rahman, T. S.; Chen, D. A. CO-Induced Diffusion of Ni Atoms to the Surface of Ni−Au Clusters on $TiO_2$(110). *J. Phys. Chem. C* **2011**, *115*, 11112−11123.
(129) Tenney, S. A.; Ratliff, J. S.; Roberts, C. C.; He, W.; Ammal, S. C.; Heyden, A.; Chen, D. A. Adsorbate-Induced Changes in the Surface Composition of Bimetallic Clusters: Pt−Au on $TiO_2$(110). *J. Phys. Chem. C* **2010**, *114*, 21652−21663.
(130) Croy, J. R.; Mostafa, S.; Hickman, L.; Heinrich, H.; Cuenya, B. R. Bimetallic Pt−Metal Catalysts for the Decomposition of Methanol: Effect of Secondary Metal on the Oxidation State, Activity, And Selectivity of Pt. *Appl. Catal., A* **2008**, *350*, 207−216.
(131) Cuenya, B. R.; Ono, L. K.; Croy, J. R.; Naitabdi, A.; Heinrich, H.; Zhao, J.; Alp, E. E.; Sturhahn, W.; Keune, W. Structure and Phonon Density of States of Supported Size-Selected $^{57}$FeAu Nanoclusters: A Nuclear Resonant Inelastic X-ray Scattering Study. *Appl. Phys. Lett.* **2009**, *95*, 143103−3.
(132) Roldan Cuenya, B.; Croy, J. R.; Ono, L. K.; Naitabdi, A.; Heinrich, H.; Keune, W.; Zhao, J.; Sturhahn, W.; Alp, E. E.; Hu, M. Phonon Density of States of Self-Assembled Isolated Fe-Rich Fe−Pt Alloy Nanoclusters. *Phys. Rev. B* **2009**, *80*, 125412.
(133) Naitabdi, A.; Ono, L. K.; Behafarid, F.; Cuenya, B. R. Thermal Stability and Segregation Processes in Self-Assembled Size-Selected $Au_xFe_{1-x}$anoparticles Deposited on $TiO_2$(110): Composition Effects. *J. Phys. Chem. C* **2009**, *113*, 1433−1446.
(134) Hasché, F.; Oezaslan, M.; Strasser, P. Activity and Structure of Dealloyed $PtNi_3$ Nanoparticle Electrocatalyst for Oxygen Reduction Reaction in PEMFC. *ECS Trans.* **2011**, *41*, 1079−1088.
(135) Yang, R. Z.; Bian, W. Y.; Strasser, P.; Toney, M. F. Dealloyed $PdCu_3$ Thin Film Electrocatalysts for Oxygen Reduction Reaction. *J. Power Sources* **2013**, *222*, 169−176.
(136) Yu, C. F.; Holby, E. F.; Yang, R. Z.; Toney, M. F.; Morgan, D.; Strasser, P. Growth Trajectories and Coarsening Mechanisms of Metal Nanoparticle Electrocatalysts. *ChemCatChem* **2012**, *4*, 766−770.
(137) Tuaev, X.; Strasser, P. Small Angle X-ray scattering (SAXS) Techniques for Polymer Electrolyte Membrane Fuel Cell Characterisation. In *Polymer Electrolyte Membrane and Direct Methanol Fuel Cell Technology: In Situ Characterization Techniques for Low Temperature Fuel Cells*; Roth, C., Hartnig, C., Eds.; Woodhead Publishing Series in Energy 31: Cambridge, U.K., 2012; Vol. 2.
(138) Anniyev, T.; Ogasawara, H.; Ljungberg, M. P.; Wikfeldt, K. T.; MacNaughton, J. B.; Naslund, L.-A.; Bergmann, U.; Koh, S.; Strasser, P.; Pettersson, L. G. M.; et al. Complementarity between High-Energy Photoelectron and L-Edge Spectroscopy for Probing the Electronic Structure of 5d Transition Metal Catalysts. *Phys. Chem. Chem. Phys.* **2010**, *12*, 5694−5700.
(139) Russell, A. E.; Rose, A. X-ray Absorption Spectroscopy of Low Temperature Fuel Cell Catalysts. *Chem. Rev.* **2004**, *104*, 4613−4636.
(140) Kiely, C. Electron Microscopy: New Views of Catalysts. *Nat. Mater.* **2010**, *9*, 296−297.
(141) Yu, Z.; Zhang, J.; Liu, Z.; Ziegelbauer, J. M.; Xin, H.; Dutta, I.; Muller, D. A.; Wagner, F. T. Comparison between Dealloyed $PtCo_3$ and $PtCu_3$ Cathode Catalysts for Proton Exchange Membrane Fuel Cells. *J. Phys. Chem. C* **2012**, *116*, 19877−19885.
(142) Mazumder, V.; Chi, M.; More, K. L.; Sun, S. Synthesis and Characterization of Multimetallic Pd/Au and Pd/Au/FePt Core/Shell Nanoparticles. *Angew. Chem., Int. Ed.* **2010**, *49*, 9368−9372.
(143) Chen, S.; Ferreira, P. J.; Sheng, W.; Yabuuchi, N.; Allard, L. F.; Shao-Horn, Y. Enhanced Activity for Oxygen Reduction Reaction on "$Pt_3Co$" Nanoparticles: Direct Evidence of Percolated and Sandwich-Segregation Structures. *J. Am. Chem. Soc.* **2008**, *130*, 13818−13819.
(144) Chen, S.; Sheng, W.; Yabuuchi, N.; Ferreira, P. J.; Allard, L. F.; Shao-Horn, Y. Origin of Oxygen Reduction Reaction Activity on "$Pt_3Co$" Nanoparticles: Atomically Resolved Chemical Compositions and Structures. *J. Phys. Chem. C* **2009**, *113*, 1109−1125.
(145) Wang, D.; Yu, Y.; Xin, H. L.; Hovden, R.; Ercius, P.; Mundy, J. A.; Chen, H.; Richard, J. H.; Muller, D. A.; DiSalvo, F. J.; et al. Tuning Oxygen Reduction Reaction Activity via Controllable Dealloying: A

Model Study of Ordered $Cu_3Pt$/C Intermetallic Nanocatalysts. *Nano Lett.* **2012**, *12*, 5230−5238.
(146) Carlton, C. E.; Chen, S.; Ferreira, P. J.; Allard, L. F.; Shao-Horn, Y. Sub-Nanometer-Resolution Elemental Mapping of "$Pt_3Co$" Nanoparticle Catalyst Degradation in Proton-Exchange Membrane Fuel Cells. *J. Phys. Chem. Lett.* **2011**, *3*, 161−166.
(147) Heggen, M.; Oezaslan, M.; Houben, L.; Strasser, P. Formation and Analysis of Core−Shell Fine Structures in Pt Bimetallic Nanoparticle Fuel Cell Electrocatalysts. *J. Phys. Chem. C* **2012**, *116*, 19073−19083.
(148) Forty, A. J. Corrosion Micromorphology of Noble Metal Alloys and Depletion Gilding. *Nature* **1979**, *282*, 597−598.
(149) Pareek, A.; Borodin, S.; Bashir, A.; Ankah, G. N.; Keil, P.; Eckstein, G. A.; Rohwerder, M.; Stratmann, M.; Gründer, Y.; Renner, F. U. Initiation and Inhibition of Dealloying of Single Crystalline $Cu_3Au$ (111) Surfaces. *J. Am. Chem. Soc.* **2011**, *133*, 18264−18271.
(150) Renner, F. U.; Ankah, G. N.; Pareek, A. In-Situ Surface-Sensitive X-ray Diffraction Study on the Influence of Iodide over the Selective Electrochemical Etching of $Cu_3Au$ (111). *Surf. Sci.* **2012**, *606*, L37−L40.
(151) Ankah, G. N.; Pareek, A.; Cherevko, S.; Topalov, A. A.; Rohwerder, M.; Renner, F. U. The Influence of Halides on the Initial Selective Dissolution of $Cu_3Au$ (111). *Electrochim. Acta* **2012**, *85*, 384−392.
(152) Sieradzki, K.; Corderman, R. R.; Shukla, K.; Newman, R. C. Computer Simulation of Corrosion: Selective Dissolution of Binary Alloys. *Philos. Mag. A* **1989**, *59*, 713−746.
(153) Rugolo, J.; Erlebacher, J.; Sieradzki, K. Length Scales in Alloy Dissolution and Measurement of Absolute Interfacial Free Energy. *Nat. Mater.* **2006**, *5*, 946−949.
(154) Maillard, F.; Dubau, L.; Durst, J.; Chatenet, M.; André, J.; Rossinot, E. Durability of $Pt_3Co$/C Nanoparticles in a Proton-Exchange Membrane Fuel Cell: Direct Evidence of Bulk Co Segregation to the Surface. *Electrochem. Commun.* **2010**, *12*, 1161−1164.
(155) Marcu, A.; Toth, G.; Srivastava, R.; Strasser, P. Preparation, Characterization and Degradation Mechanisms of PtCu Alloy Nanoparticles for Automotive Fuel Cells. *J. Power Sources* **2012**, *208*, 288−295.
(156) Xin, H. L.; Mundy, J. A.; Liu, Z.; Cabezas, R.; Hovden, R.; Kourkoutis, L. F.; Zhang, J.; Subramanian, N. P.; Makharia, R.; Wagner, F. T.; et al. Atomic-Resolution Spectroscopic Imaging of Ensembles of Nanocatalyst Particles Across the Life of a Fuel Cell. *Nano Lett.* **2012**, *12*, 490−497.
(157) Dubau, L.; Durst, J.; Maillard, F.; Guétaz, L.; Chatenet, M.; André, J.; Rossinot, E. Further Insights into the Durability of $Pt_3Co$/C Electrocatalysts: Formation of "Hollow" Pt Nanoparticles Induced by the Kirkendall Effect. *Electrochim. Acta* **2011**, *56*, 10658−10667.
(158) Yin, Y. D.; Rioux, R. M.; Erdonmez, C. K.; Hughes, S.; Somorjai, G. A.; Alivisatos, A. P. Formation of Hollow Nanocrystals through the Nanoscale Kirkendall Effect. *Science* **2004**, *304*, 711−714.
(159) Aldinger, F. Controlled Porosity by an Extreme Kirkendall Effect. *Acta Metall. Mater.* **1974**, *22*, 923−928.
(160) Fan, H. J.; Gösele, U.; Zacharias, M. Formation of Nanotubes and Hollow Nanoparticles Based on Kirkendall and Diffusion Processes: A Review. *Small* **2007**, *3*, 1660−1671.
(161) Kirkendall, E.; Thomassen, L.; Uethegrove, C. Rates of Diffusion of Copper and Zinc in Alpha Brass. *Trans. AIME*; **1939**; Vol. *133*, p 186.
(162) Henkes, A. E.; Vasquez, Y.; Schaak, R. E. Converting Metals into Phosphides: A General Strategy for the Synthesis of Metal Phosphide Nanocrystals. *J. Am. Chem. Soc.* **2007**, *129*, 1896−1897.
(163) Yin, Y.; Erdonmez, C. K.; Cabot, A.; Hughes, S.; Alivisatos, A. P. Colloidal Synthesis of Hollow Cobalt Sulfide Nanocrystals. *Adv. Funct. Mater.* **2006**, *16*, 1389−1399.
(164) Casero, E.; Alonso, C.; Martin-Gago, J. A.; Borgatti, F.; Felici, R.; Renner, F.; Lee, T. L.; Zegenhagen, J. Nitric-Oxide Adsorption and Oxidation on Pt(111) In Electrolyte Solution under Potential Control. *Surf. Sci.* **2002**, *507−510*, 688−694.
(165) Sieradzki, K.; Dimitrov, N.; Movrin, D.; McCall, C.; Vasiljevic, N.; Erlebacher, J. The Dealloying Critical Potential. *J. Electrochem. Soc.* **2002**, *149*, B370−B377.
(166) Smith, M. C.; Gilbert, J. A.; Mawdsley, J. R.; Seifert, S.; Myers, D. J. In Situ Small-Angle X-ray Scattering Observation of Pt Catalyst Particle Growth During Potential Cycling. *J. Am. Chem. Soc.* **2008**, *130*, 8112−8113.
(167) Mathew, P.; Meyers, J. P.; Srivastava, R.; Strasser, P. Analysis of Surface Oxidation on Pt and Pt Core−Shell Electrocatalysts for PEFCs. *J. Electrochem. Soc.* **2012**, *159*, B554−B563.
(168) Jirkovský, J. S.; Panas, I.; Romani, S.; Ahlberg, E.; Schiffrin, D. J. Potential-Dependent Structural Memory Effects in Au−Pd Nanoalloys. *J. Phys. Chem. Lett.* **2012**, *3*, 315−321.
(169) Kongkanand, A.; Wagner, F. High Activity Dealloyed Pt Fuel Cell Catalysts. *U.S. Department of Energy, Energy Efficiency and Renewable Energy, Annual Merit Review meeting*, presentation A.10 Catalysts; Arlington, VA, May 2013; http://www.hydrogen.energy.gov/annual_review13_fuelcells.html#catalysts or pdf available at http://www.hydrogen.energy.gov/pdfs/review13/fc087_kongkanand_2013_o.pdf.